Universidad de Concepción
Dirección de Postgrado
Facultad de Ciencias Físicas y Matemáticas
Programa de Magíster en Ciencias mención Física

En busca de Poblaciones Múltiples en NGC 7099 usando fotometría Washington.
(Searching for multiple populations in NGC 7099 using Washington Photometry)

Tesis para optar al grado de Magíster en Ciencias mención Física

Heinz Ernesto Frelijj Rubilar
Concepción - Chile
2017

Profesor Guía: Douglas Geisler
Departamento de Astronomía
Facultad de Ciencias Físicas y Matemáticas
Universidad de Concepción

1   Acknowledgements

To my family, because they always beared that I arrive at late hours, and always waited for me to finish my work to go out with them for vacations.

To my friends, because they give me relaxing moments when I most needed them.

To my partners, because they always had a good idea to solve problems with the work.

To my workgroup "PopStars" because they guided me during all this process.

To my professors, because they teached me almost all that I know in Astronomy.

And specially to my Advisor, because he always had time for my questions, meetings and my unexpected problems.
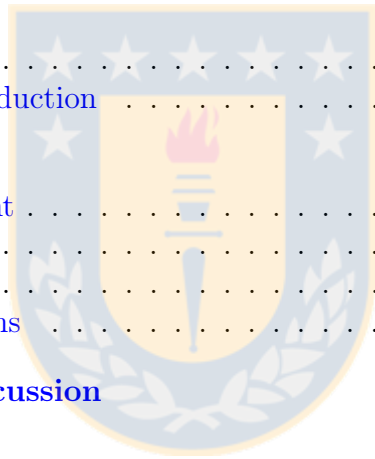
2   Abstract

Recently, the classical definition of globular clusters as simple stellar populations was overturned due to the discovery of the "multiple populations" (MP). These are stars with different ages and/or chemical properties within the same globular cluster(GC). However, our knowledge of the extent of this phenomenon and its characteristics is still lacking greatly observationally. It is important to study as many GCs as possible to determine whether or not they have MP, and characterize any MP found with respect to color and/or abundance distribution, radial distribution within the cluster, etc. The Washington filter system has proved to be useful to find MPs thanks mainly to the UV-sensitivity and high efficiency of the C filter, which contains all of the strong molecular bands most affected in red giants by the MP phenomenon. NGC 7099 (M30) is the second GC being searched for MPs using this system, and here we explain how we apply it to find them. We have conducted a search for MPs in the Galactic GC NGC 7099 using the Swope 1m telescope at Las Campanas Observatory. We discuss in detail the photometry we obtained and its analysis with respect to MP. In particular, we pay careful attention to our photometric error analysis, performing extensive addstar experiments. Our evidence indicates that NGC 7099 has MPs, as witnessed by an intrinsic color spread on the red giant branch. And contrary to the expected results, we find that the most likely first generation stars are more spatially concentrated than their second generation counterparts. We briefly discuss a possible explanation for this phenomenon.

Contents

List of Figures

List of Tables

3 Introduction

3.1 Basic Concepts

3.1.1 Star Clusters

Star Clusters are groups of stars gravitationally bound. Their composition, age and number of stars will vary depending of their type. In our galaxy there are two types of Star Clusters: Open Clusters and Globular Clusters.

Star clusters are formed in Giant Molecular Clouds composed principally of H_2. Once the first stars begin to form, the Hydrogen near them is illuminated and ionized (ionized Hydrogen is called HII). This indicates that only a little part of the gas is used to form stars, and all the remnant gas that is heated is rapidly blown away from the protocluster. After this stage most of the stars remain together due to their collective gravity, but there are some that escape due to the exchange of energy of the stars inside the protocluster. The remaining stars become gravitationally bound, forming an "Open Cluster".

Subsequent survival depends mostly on the cluster mass. If sufficiently massive, the cluster can survive for roughly a Hubble time. Our Galaxy produced a very large number of very massive clusters early in its infancy which still survive today, which are called "Globular Clusters".
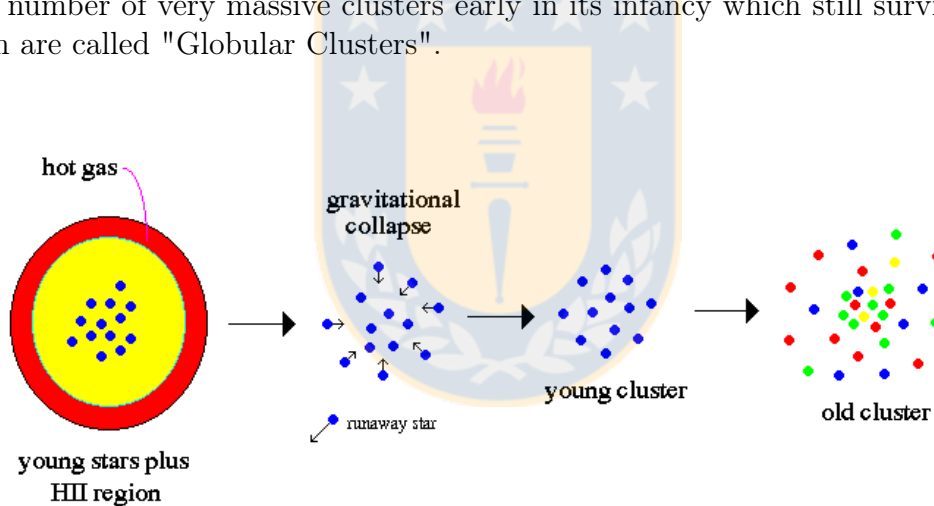
Figure 1: Stages of formation for star clusters. Source:http://abyss.uoregon.edu

Open Clusters

An Open Cluster is a group of stars orbiting in the disk of the galaxy, normally from a few hundred up to a few thousand stars, that share the same Giant Molecular Cloud as a place of birth. Since this cloud is believed to be homogeneous and star formation proceeds rapidly, all of the stars formed have roughly the same age and the same chemical composition(see "Stellar Populations"). The name "Open" is due to their loose appearance, because the stars inside them are relatively loosely bound to each other and there are relatively small number of stars compared to the more massive globular clusters ($10 - 10^3$ solar masses versus $10^4 - 10^6$ solar masses), giving an open cluster an irregular form. They are found in Spiral and Irregular galaxies, in which active star formation is occurring. Open Clusters are considered as young objects compared to globulars. Most are less than a few hundred million years old,

and it is common to find gas from molecular clouds surrounding them, meaning that there are still stars being formed there. Their relatively young age is graphically demonstrated by the presence of blue, massive stars, that have the shortest lifetimes, indicating a recent formation episode. Open clusters are important objects in the study of stellar evolution, because the stars are all of very similar age and chemical composition (see section "Stellar populations"), and the effects of other more subtle variables on the properties of stars are much more easily studied than they are for isolated stars.

In addition, Open Clusters tend to be dispersed before most of their stars reach the end of their lives, because their small gravitational binding energy allows to the cluster to become disrupted by close encounters with other clusters and clouds of gas as they orbit in the dense Galactic disk. They also lose members through internal close encounters. However, given sufficient mass and depending on their Galactic orbit, some open clusters can survive for a very long time, with a few as old as 8 Gyr.

Figure 2: The Pleiades, one of the best known Open Clusters. Source: www.bibliotecapleyades.net

Globular Clusters

Globular Clusters are very old groups of stars orbiting mainly in the Halo of the Galaxy, but we can found them also in the thick disk and the bulge. They orbit in generally random directions, with no net rotation. They are tightly gravitationally bounded, giving to the cluster a spherical or "globular" shape. They are composed of hundreds of thousands or millions of old, low mass, low metal content stars, with higher density towards the center of the cluster.

One of the most notable characteristics of Globular Cluster are their ages, because they are among the oldest objects in the universe, with the oldest oldest being approximately 13 billion years old. This makes them extremely useful to study the age of the Universe as well as the formation of structure in it like galaxies. There are

no molecular clouds inside Globular clusters, hence there is no current star formation. This fact, alongside their age explains the reason of why there are no blue stars, which are the brightest ones in the optical wavelength, and the most massive. Because of this they evolve more rapidly than low-mass stars because they develop the necessary central pressures and temperatures for hydrogen fusion sooner(Kaufmann, W.J., Universe, 3rd Edition). The brightest stars in globular clusters are instead red giants.

There is a strong debate about the formation scenarios of Globular Clusters. One of the most accepted formation theories is the one described in the beginning of "Stars Clusters" section, but some studies, like Ideta & Makino (2004) present evidence of the formation of ω Centauri by Tidal Stripping of a Dwarf Galaxy. However, it is now recognized that ω Cen is a very unusual object (the most massive GC in the Galaxy) and its formation and evolution is not typical.

Globular Clusters were for a very long time considered as Simple Stellar Populations (see "Stellar populations"), but different kinds of studies during the last decade showed the opposite, originating the term "Multiple Populations" explained later in this work.
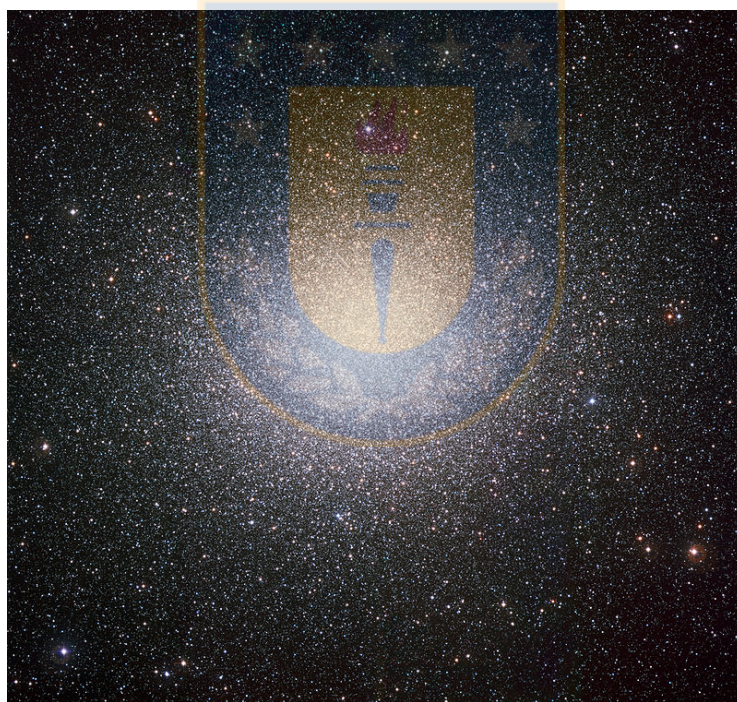
Figure 3: ω Centauri, the most massive globular cluster in the Galaxy. Source: http://earthsky.org

3.1.2   Observational Techniques

Studies like the search for Multiple populations requires observational evidence, and for that we need to use appropriate observational techniques and understand how they work in order to properly interpret the data and arrive at robust results. There are basically two types of techniques: Spectroscopy and Photometry.

Spectroscopy

Spectroscopy is a common method to study the Universe. This method consist in passing light through a slit and a prism to see its spectrum. An instrument called a spectrograph realizes this action. There are three types of spectra, continuous, absorption and emission.

A continuous spectrum is simply the light in all wavelengths, like a rainbow, having no apparent breaks or gaps throughout its wavelength range.

An emission spectrum consists in discrete bright lines(called emission lines) from the continuous spectrum seen while heating a gas and passing its radiation through the spectrograph.

An absorption spectrum consists in a continuous spectrum with dark lines (called absorption lines) seen while passing continuous radiation through a cold gas and then a spectrograph. Both the emission and absorption lines are produced by the presence of different elements at different physical conditions (temperature, gravity, etc.)(Eric Chaisson, Steve Mcmillan,(2004) Astronomy Today, Unit 4)
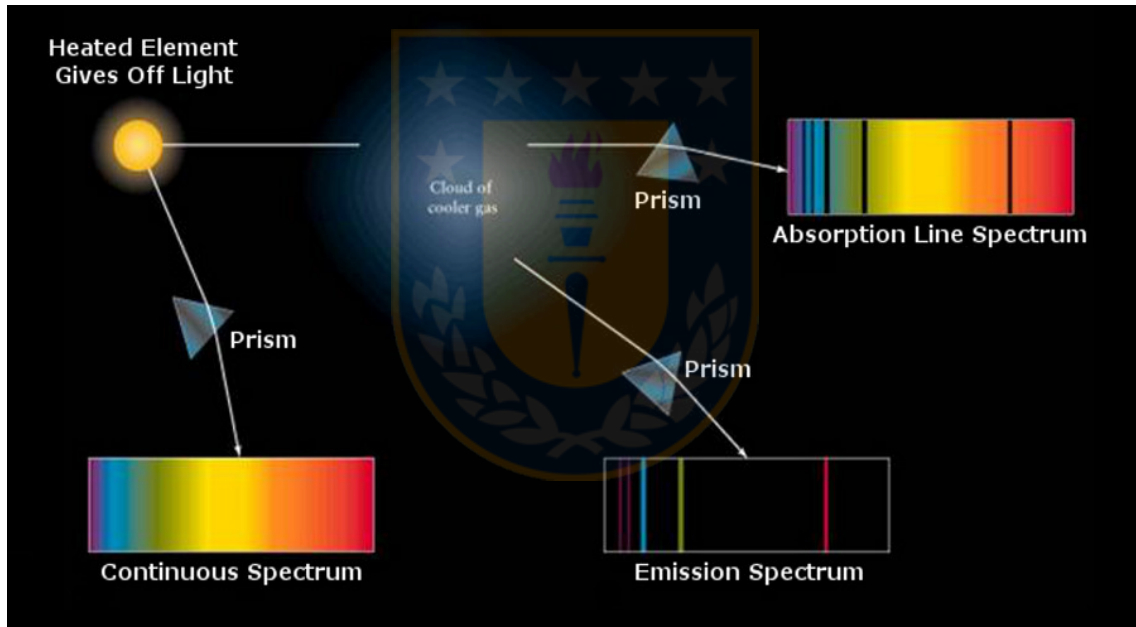
Figure 4: Different types of spectra and how they are produced. Source: http://www-revista.iaa.es

Photometry

Photometry is the science of measuring the flux within a limited wavelength range that we receive from celestial objects. The wavelength range is generally isolated using a filter and then imaging through this filter. The flux in a star is the sum of the star's contribution over all pixels illuminated by it, after subtracting the contribution from the sky background.

A simple kind of photometry consist in using a circular measuring aperture and a concentric sky annulus in which to determine the average sky background, this is called Aperture Photometry, figure 5 illustrates this. But this method present problems with varying background due to the difficulty of measuring the true sky level(i.e.

crowded fields).(W. Romanishin. An introduction to astronomical Photometry using CCDs).A more serious problem, especially in the very crowded central regions of a globular cluster, is that of image crowding, whereby two distinct stars are not well resolved in the image, thus causing the light of each to affect the measurement of the flux from the other.
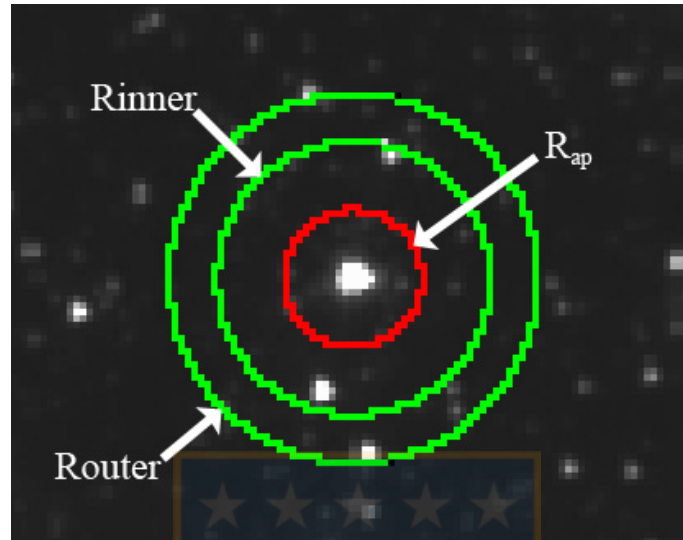
Figure 5: Aperture photometry parameters: standard aperture (red) and local background annulus (green). Source: WISE data processing page.

One useful technique to circumvent this problem is to determine a Point Spread Function (PSF) based in isolated stars of the frame. A PSF is the shape of the CCD image of a point source of light. In astronomy, the dominant determinant of the PSF is smearing caused by the passage of starlight through the Earth's turbulent atmosphere. This smearing is called seeing.

Figure 6: A graphic explanation of how determining a good Point Spread Function can characterize the light profile of stars in crowded fields. Source: Own elaboration

With a well determined PSF, the stars can be measured one by one, starting with the brightest, but then digitally subtracting(by properly shifting and scaling the image PSF) each star from the image as it is measured. This leaves fewer star to mess up the sky and cause contamination for the fainter stars. This technique

is known as PSF Photometry.(W. Romanishin. An introduction to astronomical Photometry using CCDs)

Photometry measurements are combined with the use of colored filters in order to limit the wavelength they measure. Different filters, sensitive to different wavelength regions, yield different information for each star. A commonly used technique is to calculate the difference between the flux in two or more filters to make a color and plot it versus the flux in a filter. This graph is called Color-Magnitude Diagram (CMD).

CMDs of clusters contain a vast amount of information concerning the stars, stellar evolution and the cluster itself; e.g. its distance, age, reddening, composition, etc.
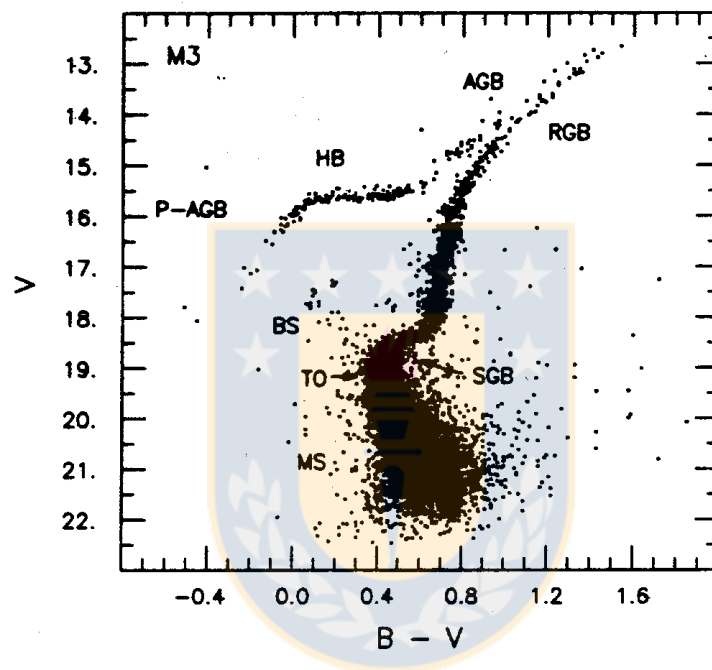
Figure 7: Color-Magnitude Diagram with all its parts. Source: Annual Review of Astronomy And Astrophysics, Vol 26, 1988.

The CMD is divided in the following parts:

Main Sequence(MS): Part of the CMD where the star stays almost all of its life, where stars fuse H into He in their centers.

Turn off Point(TO): Part of the CMD where a star leaves the main sequence after the exhaustion of all its core H.

Subgiant Branch(SGB): Part of the CMD where the star is increasing its size to become later a giant, developing a H-burning shell.

Red Giant Branch(RGB): Part of the CMD where a star stays before helium ignition. At this stage the star is red due to its expanded size which cools the outer layers and is luminous despite its coolness due to its large surface area. The energy source is still H shell burning.

Horizontal Branch(HB): Part of the CMD where stars are powered by helium fusion in the core. It has higher temperature and lesser luminosity than an upper RGB star.

Asymptotic Giant Branch(AGB): Part of the CMD where the star inhabits after core He exhaustion. An AGB star can have both H and He burning shells, causing

various instabilities, leading to the ejection of its outer layers to leave a core of carbon and oxygen, leaving a white dwarf. (Astronomy Today/Chaisson & Mcmillan-5th edition)

3.1.3   Stellar Populations

A Stellar Population refers to a group of stars that resemble each other in spatial distribution, chemical composition, kinematics and/or age.

Simple Stellar Populations consists of stars born at the same time and having the same initial element composition. For example, Open Clusters are Simple Stellar Populations, since they are composed of stars with the same age and initial abundance, as confirmed by a number of observational studies. As said in the last section, Globular Clusters were also long considered as Simple Stellar Populations. But over recent years, new investigations have refuted this, finding evidence of different chemical abundances inside Globular Clusters for the majority, if not all, of them. Thus, a new definition was required: Multiple Populations, indicating that there are not only a single population of stars like open clusters, but two or more populations of stars that do not share the same age and/or initial composition. Thus, the recognition of MPs in globular clusters has revolutionized the understanding of them, making them at the same time both more complicated as well as more interesting.

3.2   Multiple Populations

3.2.1   Formation scenarios for MPs

There are various formation scenarios for GCs that try to explain MPs (i.e. Carretta et al. (2010), D'Ercole et al. (2008), Hénault-Brunet et al. (2015), Renzini et al. (2015), among others), but there is no consensus about the true scenario because the majority are in conflict with one or more observational constraints or can't explain some processes. Valcarce and Catelan(2011) make an overview of some scenarios, and present a "toy model" dividing GCs by their initial mass to explain each formation process. The formation process has the same begining for all cases:

1) A GC begins with the gravitational collapse of a cloud where first generation (FG) stars are formed following a homogeneous distribution throughout the GC. They are initially embedded inside the interstellar medium (ISM) gas that was not used up to form stars. These are indeed a simple stellar population.

2) The gas is distributed over a larger volume than required to trigger a new local fragmentation process to form a new generation of stars, decreasing the local gas pressure for the same potential well. This causes that the remaining gas starts to fall again into the center of the cluster. Massive stars begin to eject at high velocities their envelopes, which then collide with the falling gas, decreasing the speed of the expanding massive star ejecta and the infalling gas.

From here, the process is differentiated according to the GC initial mass.

Low-mass Progenitor Structures

2b) Low-mass Progenitor Structures (PS) are unable to retain the FG massive star ejecta because of their shallower potential well, and the consequent low velocity of the infalling primordial gas. For the same reason, the PS core does not contain enough material to transform all the kinetic energy of massive star ejecta into thermal energy. The formation of a viable star-forming cloud in the core is thus inhibited.

3) FG core-collapse SNe explosions begin, which completely clean the PS of the remaining primordial gas.

4) In this case, SG stars are formed only with (diluted) gas ejected by super-AGB and/or AGB stars, with the chemical composition of the ejecta depending in detail on the stellar mass.

5) This is potentially a continuous process, with renewed cleansing of the intracluster gas taking place after each new star formation event.

Figure 8: Low-mass PS scenario according to Valcarce and Catelan(2011). Stages are detailed in text. Source: Valcarce and Catelan(2011)

Intermediate-mass Progenitor Structures

2b) Since intermediate-mass PSs have deeper gravitational potential wells than low-mass PSs, the infalling gas reaches a higher speed, and a fraction of the massive star ejecta is retained before their progenitors explode. However, in the outer parts of the PS the massive star ejecta are trying to escape, as the pristine gas is infalling. Additionally, in the PS core, where the primordial gas has been accumulating, the gas ejected by massive stars is slowed down, and the kinetic energy transformed into thermal energy, which delays further star formation.

3) When FG core-collapse SNe explode, their ejecta compress the center cloud, thus triggering star formation in the SG. These SG stars have been highly enriched in helium by the massive star ejecta, but at the same time are not heavily enriched in metals. Assuming that SN explosions are nearly symmetrical and that their precursors are not too close to the center, only a small fraction of the SN ejecta, which

is metal-enriched, will be mixed with the core cloud. This event also completely removes the outer mixed gas from the cluster, since the gravitational potential well is not deep enough and the mass of the outer infalling gas is insufficient to retain the SNe ejecta. Thus, SG stars will accordingly not be metal-enriched.

4) The ejecta of massive SG stars are not retained in the case of an intermediate-mass PS, because the infalling gas is only produced by intermediate-mass FG stars. If any such gas is initially retained, it will eventually be expelled by SG corecollapse SNe or FG type Ia SNe explosions, or will form but very few stars.

5) After this second cleansing of the cluster, a new cloud begins to form in the cluster center, using the intermediate mass stellar ejecta (mass lost at low velocity) from FG and SG stars. The chemical composition of this new cloud falls between both generations, as a consequence of the slope of the IMF (which favors low-mass stars) and the mass ratio of both generations. Here, the first stars of the third generation (TG) will be created.

6) These star formation and cluster ISM cleansing stages continue, with each successive stellar population becoming chemically more similar to FG stars, while at the same time less numerous.
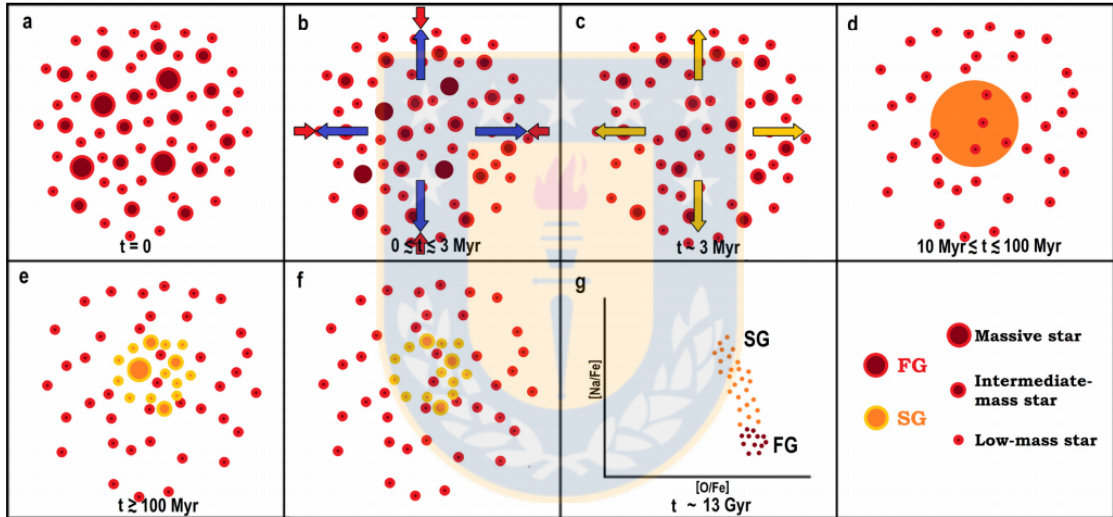

Figure 9: Intermediate-mass scenario according to Valcarce and Catelan(2011). Stages are detailed in text. Source: Valcarce and Catelan(2011)

Massive Progenitor Structures

2b) As in Intermediate mass scenario, in the PS core a cloud has been formed that is highly enriched in helium. Its material comes from massive star ejecta and a fraction of the remaining gas that was not used to form FG stars. However, in the outer part of the PS the massive star ejecta is trying to escape, while the pristine gas is infalling to the PS center with a velocity (and a total mass) that is higher than in the case of intermediate mass PSs.

3) The first core-collapse SNe explosions compress the core gas, triggering the SG star formation episode. As in Intermediate mass scenario, these SG stars are highly enriched in helium. However, in contrast to what happens in the Intermediate mass case, the deeper potential well does allow the gas in the outer part of the cloud to

be retained. Most of the SN ejecta tries to escape the cluster, merging with the infalling gas in the process. This event efficiently mixes both gas components, and delays the moment of arrival of this mixed gas to the core.

4) After a while, the highly metal-enriched material is mixed with the gas that was not used to form SG stars, creating a new cloud in the core of the cluster.

5) This cloud is also fed by SG massive stars and by both massive and intermediate-mass FG stars – and these provide the chemical ingredients that will characterize the cluster's third generation (TG) of stars.

6) With three stellar generations in the cluster, the process of star formation continues, but each time with material processed mainly by less massive stars. As a result, the newborn stars belonging to the fourth generation (4G) will have a chemical composition that is a mixture of products from the three preceding generations. In this scenario, SG and TG stars are created using only a relatively small fraction of the total mass that was used to form FG stars. In other words, subsequent stellar generations will be increasingly affected by the evolution of lower-mass stars, whose ejecta will not be chemically very different from that of the original PS gas.
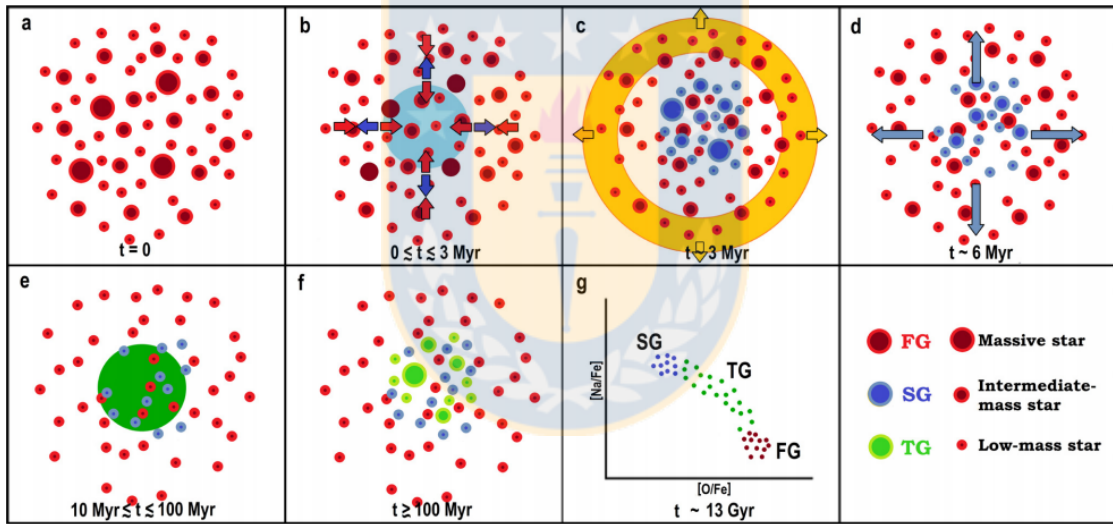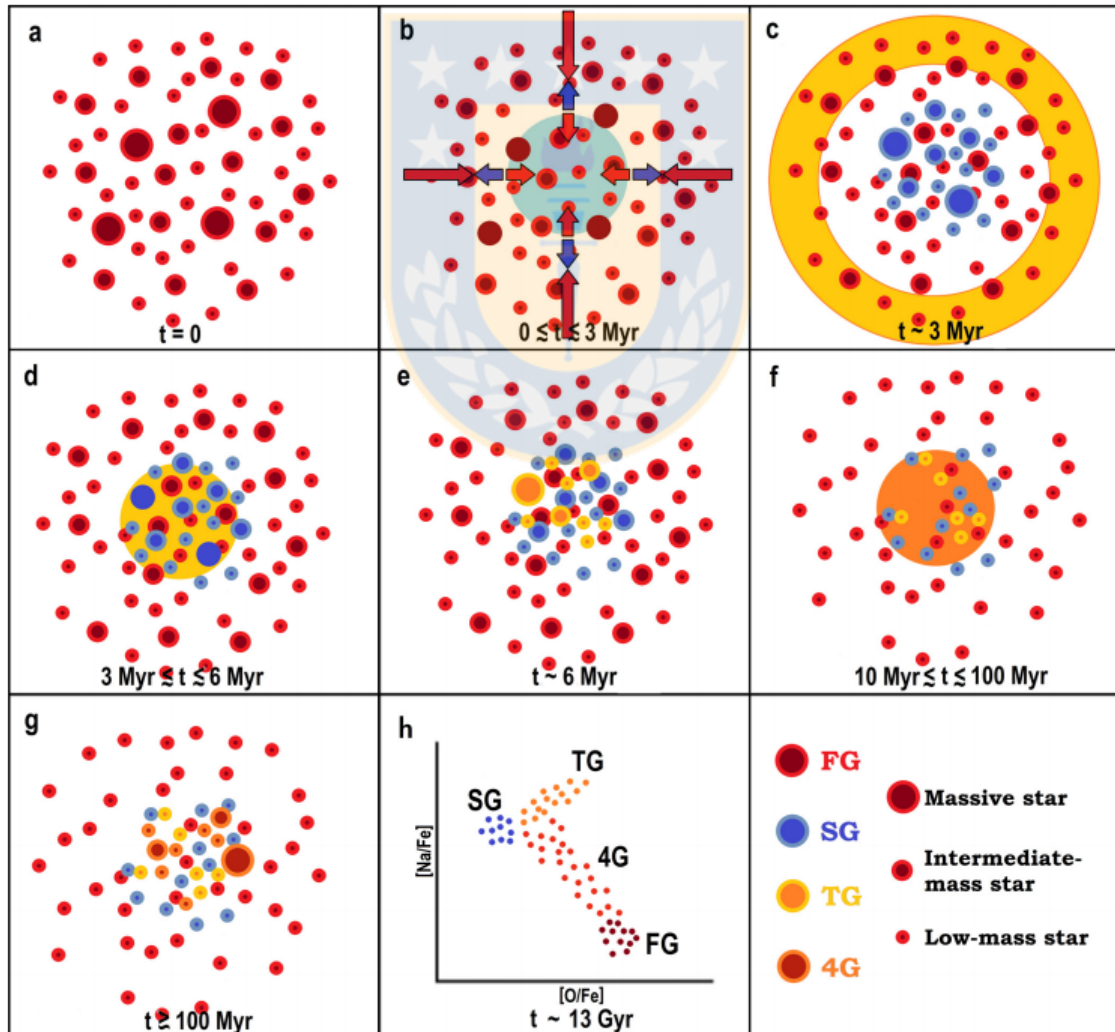

Figure 10: High-mass scenario according to Valcarce and Catelan(2011). Stages are detailed in text. Source: Valcarce and Catelan(2011)

Caretta et al.(2009) find that generally SG stars make up roughly 2/3 of the current cluster population.In order to explain the large fraction of SG stars seen now and the small amount of polluted material that can be delivered by the FG requires that the original cluster was some 10 or more times more massive than it is today, i.e. that each cluster has lost 90% or more of its initial mass. This is termed the "Mass Budget Problem". So far, no strong evidence either observational or theoretical exists for such an extreme mass loss.

Some models try to "alleviate" the mass budget problem. D'Ercole et al. (2010) postulate a different Initial Mass Function between 1G and 2G stars, with that of 2Gs being truncated at a mass close to or below ~ 8 M$\odot$, thus reducing the mass budget and avoiding supernova pollution from one 2G star to another. However, this theory remains unproved(Renzini et al. (2015)).

Actually all models require huge amounts of He enrichment which are simply not observed. "None of the proposed scenarios can explain the multiple population phenomenon, hence alternative theories are needed".(Bastian et al (2015)). However, such models serve as a useful attempt at trying to understand the nature of MPs.

In the rest of this thesis, we will refer to FG and SG stars in the above context but recognize that we are still a long way from a successful theory.

3.2.2 Abundance differences in Globular Clusters

A key feature of MPs in CGs are the light elements abundance variations between FG and SG stars. Osborn(1971) found a variation in CN among RGB stars. This was the first detection of abundance variations, long before the discovery of MPs.

A decade after, Norris (1984) found an anticorrelation between CN and CH on the RGB. Further studies, like Smith & Norris (1984) and Martell & Smith (2009) among others, proved these two abundance variations to be a feature of GC. It is interesting to mention that Martell & Smith (2009) studied the CN abundance difference not only in GC, but in Open Clusters too, but they didn't found inhomogeneities in the latter.

These were found not to be the only abundance differences: Cohen(1978) was the first one to find a difference in abundance of Na in GCs. Several years later, Cottrell & Da Costa(1981) found a correlation between CN and Na and Al. Sneden et al. (1992) found an anticorrelation between CN and O, and a correlation between CN and Na.

Following the (admittedly flawed) formation scenarios seen in the past section, the differences of chemical abundances of FG and SG stars can be explained as follow:

1) FG stars have normal levels of He, C, N, O, Na, Al and Mg, similar to field stars.

2) While the CNO cycle tends to convert their C and O into N, their Na is enriched by the $^{22}Ne(p,\gamma)^{23}Na$ reaction.(Lee (2010)), He is enriched via the CNO cycle, and in the most massive stars Al is enriched by the MgAl cycle.

3) FG intermediate-mass stars become AGB stars.

4) The primordial pollution via stellar winds of these FG intermediate-mass AGB stars provides these element abundances to the proto-stellar clouds of the SG of stars.

Comparing the spectra of a FG versus a SG star the abundance differences can be seen. The following image (figure 11) shows representative spectra of first and second

generation red giants with the same atmospheric parameters and only differing in the content of the light elements C, N, O and Na.
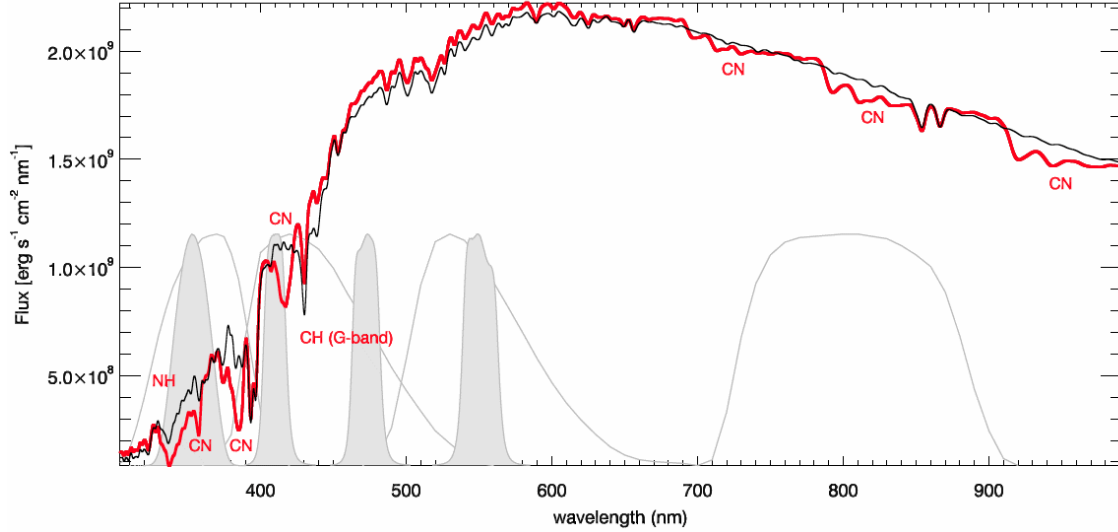

Figure 11: Comparison between the synthetic spectra of a First(black spectrum) and Second generation star(red spectrum) illustrating the variation of C, N, O and Na. Various photometric filter responses are also shown. Source: Sbordone et al (2011).

The spectra are substantially different in the molecular bands formed by these elements, particularly in the UV-blue portion of the optical. A filter covering any or all of these bands should therefore be sensitive to these varying band strengths, thus revealing MPs photometrically.

3.2.3   Evidence of Multiple Populations in Globular Clusters

A common method to find MPs with spectroscopy is to identify abundance correlation or anticorrelations between first and second generation stars. The most famous is the Na:O anticorrelation.

Carretta et al.(2009) realized a Na:O anticorrelation study Using FLAMES/GIRAFFE spectra of more than 2000 RGB stars in 19 GCs - see Figure 12. Their detections are indicated as open circles. Although they could not measure O abundances in all stars, they placed upper limits to O abundances, represented as arrows. Star-to-star error bars are indicated in each panel at the bottom-left. This evidence show that all these clusters present an Na:O anticorrelation!. However, the slope and shape of the anticorrelation varies for each cluster. This was the first convincing evidence that MPs were not just an isolated phenomenon occurring in a few special cases but instead a general, possibly universal, phenomenon found in a wide variety of GCs.
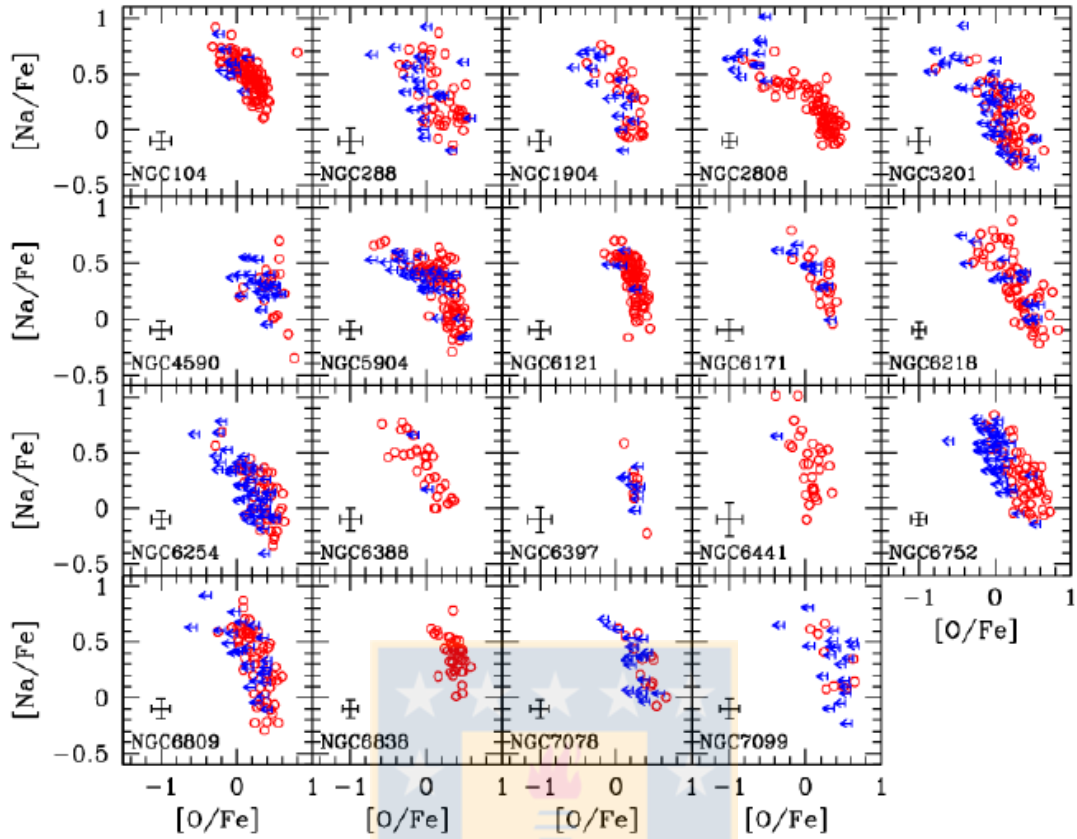
Figure 12: Na:O Anticorrelations of 19 GCs observed from Carretta et al (2009).Upper limits in O abundances are shown as arrows, detections are indicated as open circles. Source: Carretta et al (2009)

As said before, and looking figure 11, some filters facilitate the photometric study of MPs. Sometimes these are demonstrated by distinct multiple sequences, as seen below (figure 13) in the case of ω Cen, and sometimes MPs are distinguished photometrically by spread in color in a given filter combination that is significantly wider than the observational errors, indicating an intrinsic variation in abundances within the cluster.(Figure 14)
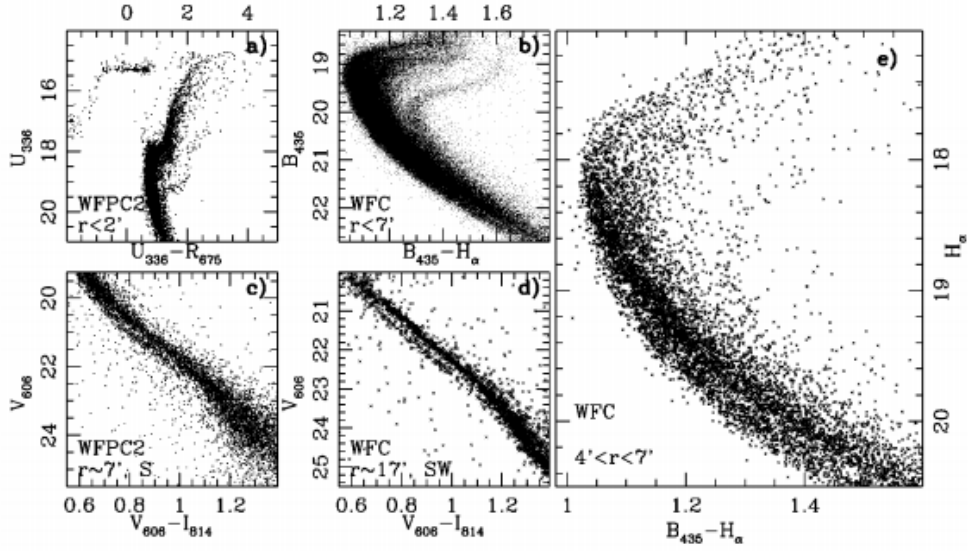
Figure 13: Color-Magnitude Diagrams of Omega Cen showing Multiple sequences, indicating the presence of MP. Source: Bedin et al. (2004).
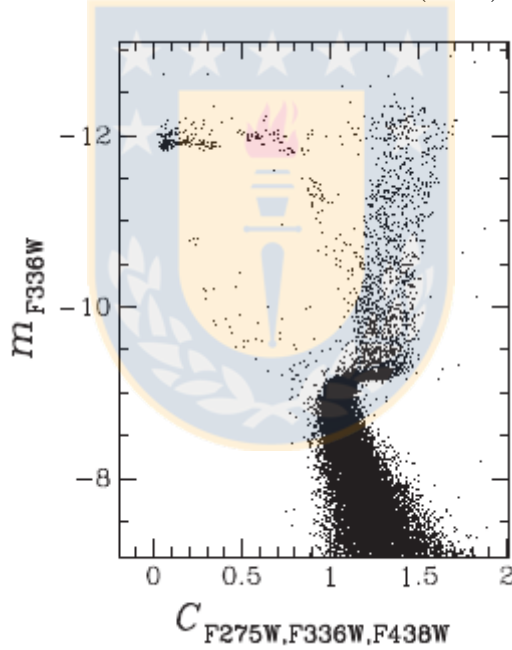
Figure 14: CMD of NGC 5986 using the "Magic trio" of filter from Piotto et al. (2015). The CMD doesn't show distinct sequences but a significantly wide RGB. Source: Piotto et al. (2015)

Piotto et al. (2015) realized a study over 57 GCs using the "Magic trio", as part of the HST GC Treasury Survey. This "magic trio" consists in a combination of three filters F275W, F336W and F438W with which Milone et al. (2013) defined a pseudo-color $C_{F275W,F336W,F438W} = (m_{F275W} - m_{F336W}) - (m_{F336W} - m_{F438W})$ that proved to be quite efficient in the separation of multiple sequences. The reason why F275W, F336W and F438W work so well is given by Milone et al. (2012): The F275W passband includes an OH molecular band, F336W an NH band, and F438W CN and CH bands, as illustrated in Figure 15.

14
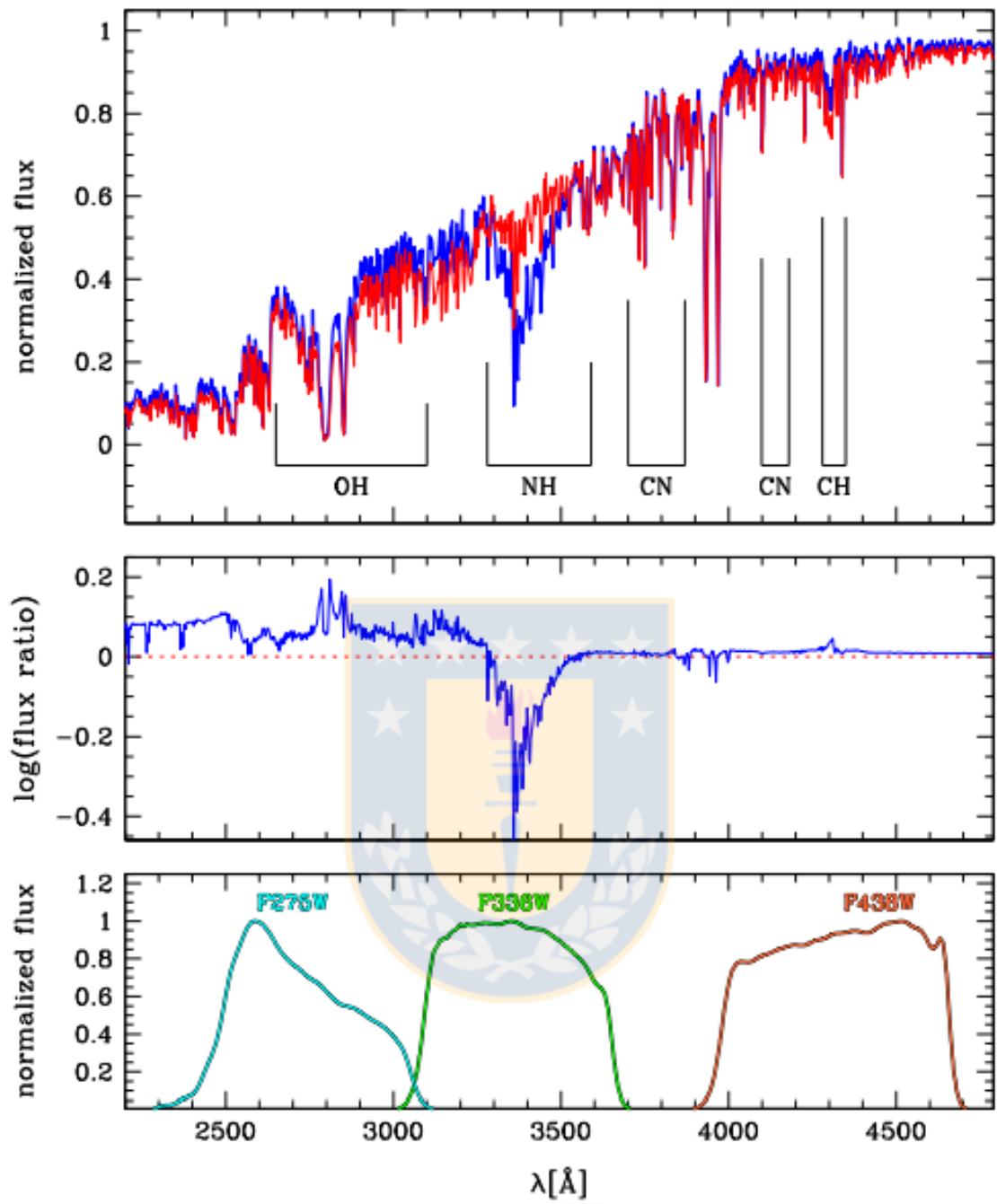
Figure 15: Upper panel: Simulated spectra of FG star(N-poor) RGBa in NGC 6752(red) and a second generation(N-rich) RGBc star (Milone et al. 2010). Middle panel: flux ratio of the two spectra reproduced in the upper panel. Lower panel: bandpasses of WFC3/UVIS with F275W, F336W, and F438W. Source: Piotto et al. (2015)

With such evidence is very tempting to say that all GCs have MPs, but Villanova et al. (2013) showed evidence suggesting that Ruprecht 106 is the first genuine old, massive GC with only a single population, thus opening new questions about the nature of GCs and MPs. Thus it is essential to investigate as many GCs as possible to determine whether or not they contain MPs and if so, what the details of their MP behavior are.
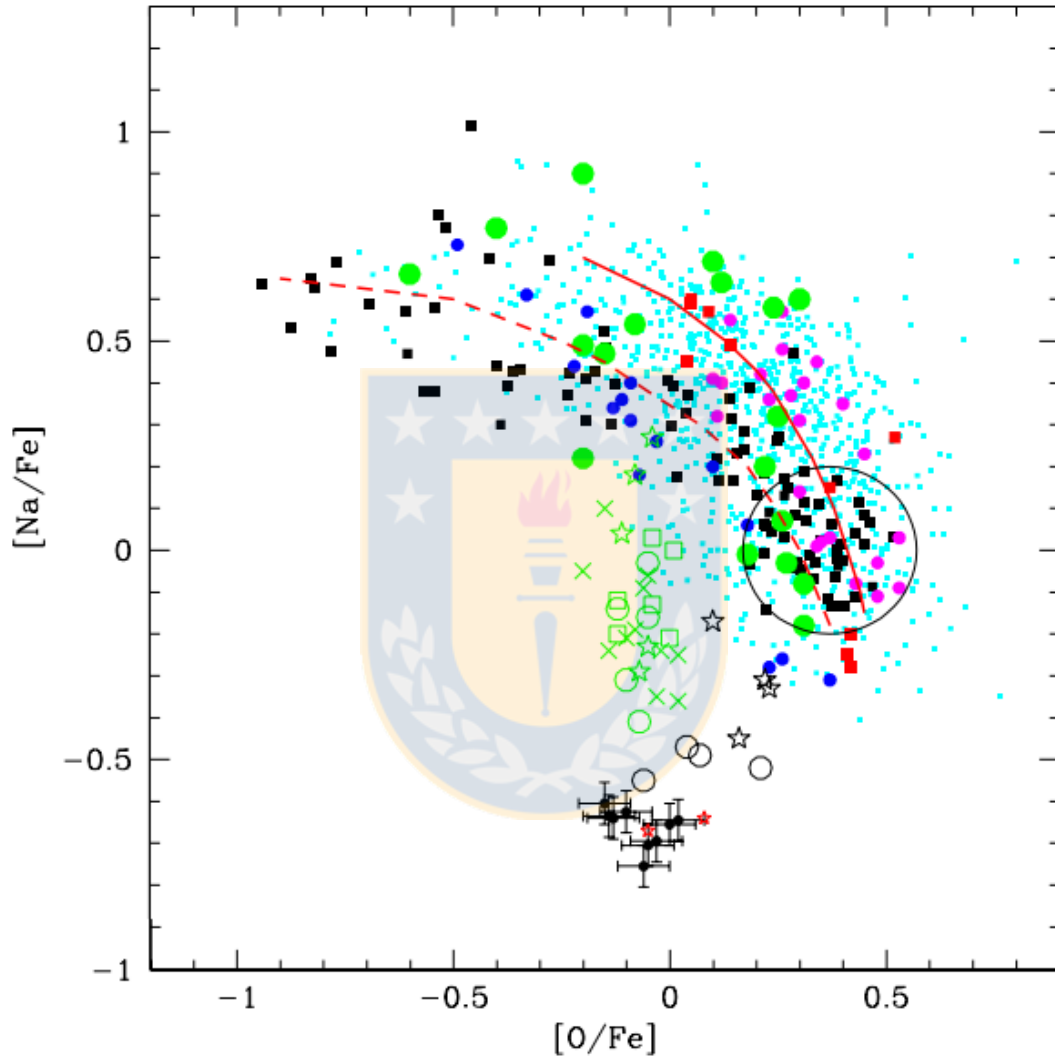
Figure 16: [Na/Fe] vs. [O/Fe] in GCs. Filled black circles and open red stars are samples from Ruprecht 106 by Villanova et al. (2013) and Brown et al. (1997) respectively, while all the other figures are samples from other clusters. The Rup 106 stars are lie within the measurement errors of the same abundance for both O and Na. Source: Villanova et al. (2013)

3.3 Washington Filter system

As discussed above, examples like Carretta et al. (2009), showed spectroscopically that all clusters they studied present a Na:O anticorrelation. Such spectroscopic studies are more accurate in general than photometry as they derive detailed abundances for a number of different species. However they are limited by the number of bright stars for which high resolution spectra of sufficient S/N can be obtained. And high resolution spectroscopy requires large telescopes with multiobject spectrographs.

As showed before, photometry using appropriate filters is another complementary way to search for Multiple Populations. While this method cannot provide the detailed abundances of spectroscopy, it allows the measurement of a much larger sample of stars simultaneously and to much fainter absolute magnitudes, with much smaller telescopes.

Examples like Bedin et al. (2004) and Piotto et al. (2015), have found strong photometric evidence of MPs through a significant spread or even a split in not only the Red Giant Branch (RGB) but in the Sub Giant Branch (SGB) or even the Main Sequence (MS).

These studies, like those with the Magic trio, are crucial to uncovering Multiple Populations. However, they do require very expensive time on big telescopes like the Hubble Space Telescope. Meanwhile, it is of great interest to explore the possibilities of uncovering Multiple Populations with ground-based photometry, especially with relatively small telescopes, proving that a given system is especially sensitive to MPs.

The Washington System developed by Canterna (1976) consist of four filters (C, M, T_1, T_2) initially developed to obtain accurate temperatures, metal abundances and a CN index for G and K giants.
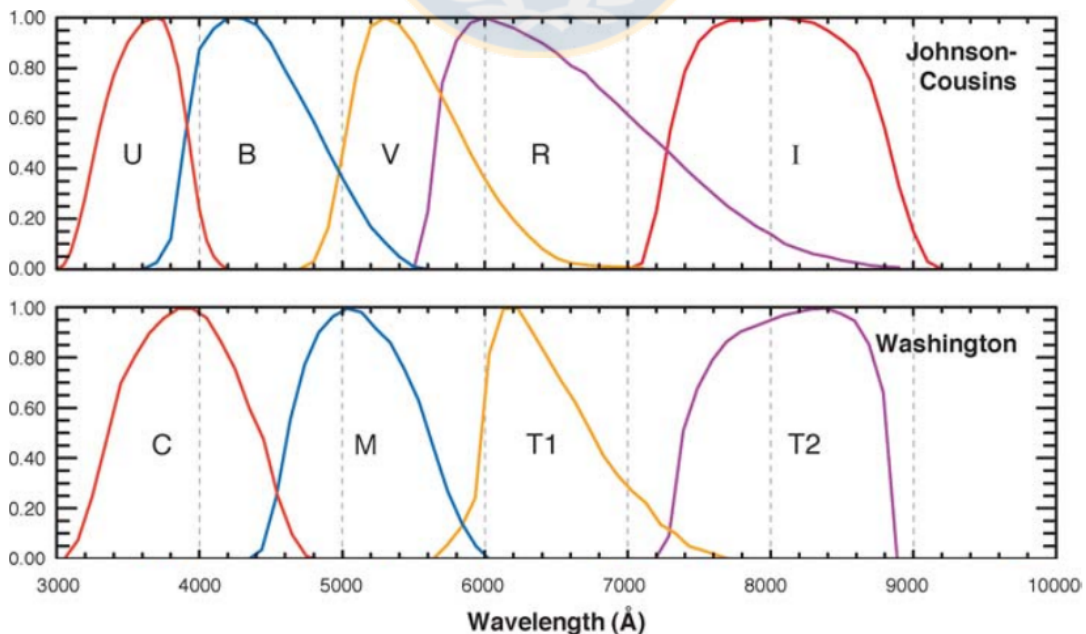

Figure 17: Comparison of the spectral response between the classic Johnson-Cousins Filter system and the Washington Filter system. Source: Bessel (2005)

The most important filter for this study is the C filter which indeed was designed to detect Multiple Populations, although at the time they were not designated as such. The C filter was added to the system to provide a measurement of CN/CH enhancements or depletions independent of the metallicity index measured by the M filter, just at the time when CN/CH variations within clusters were being discovered. The ability of ground-based C photometry to detect Multiple Populations in Globular Clusters was first explored in Cummings et al. (2014). They found that the filter was indeed very useful in this regard, given both the UV sensitivity as well as the high efficiency of this broad band (FWHM >1000 Å). The Washington C filter is very broad and covers the wide range from about 3500 - 4500 Å, where the largest flux differences exist between first and second generation stars due to the strong molecular bands of NH, CN and CH, making it very efficient for this task.

Note that the C filter covers all of the classic, very strong UV-blue bands formed by these molecules in cool giants, which are optically the brightest stars in these clusters.
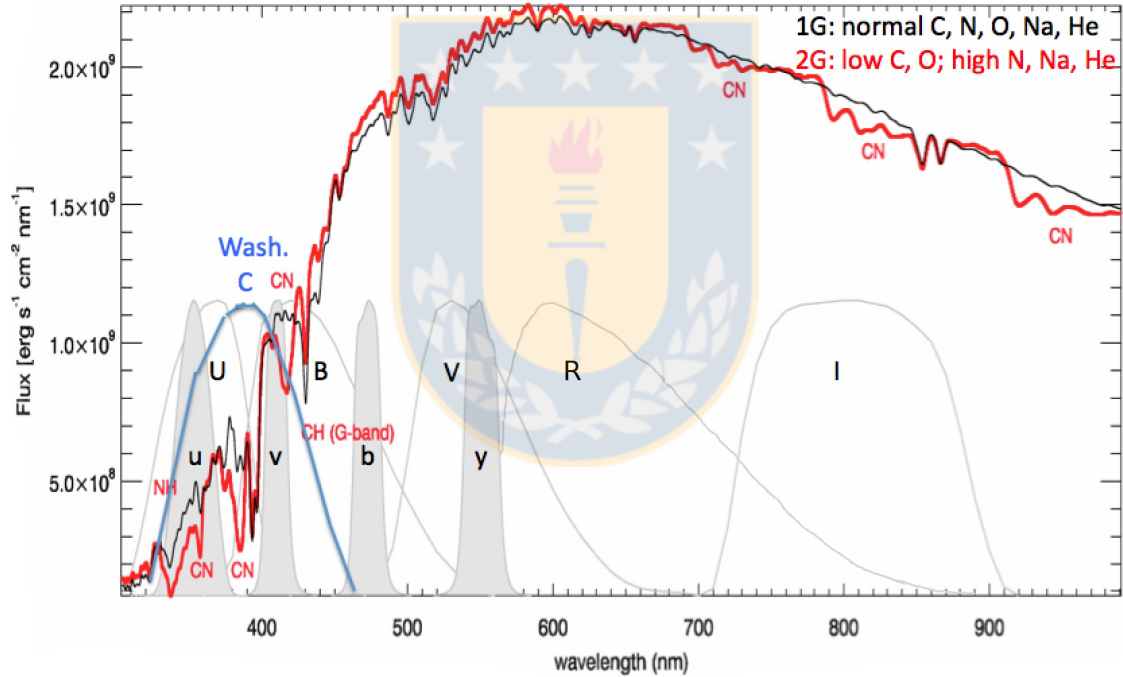
Figure 18: Modification of Figure 11 with the filter C added. The Washington C filter covers the entire region of the largest difference between 1G and 2G stars, in the UV due to the various molecular bands. Source: Cummings et al. (2014)

This filter is similar to the classical Johnson filter U, but much wider and with a higher peak transmission. It is also centered further to the red, making it less sensitive to atmospheric extinction and interstellar reddening. It is even more efficient with respect to the intermediate-band Sloan u and Stromgren u filters (Table 1). Tests at the telescope have shown that the C filter detects 3-5 times as many photons as the U filter for a typical red giant.

Filter	Central λ	FWHM (λ)	Peak Transmission	Source
Johnson U	3570	650	72.47%	1
Washington C	3850	1075	83%	1
SDSS u	3600	65.49	65.49%	1
Stromgren u	3537	278	38%	2

Table 1: Comparison of UV filters with the Washington filter C. Source: Cummings et al.(2014).

Cummings et al. (2014) Investigated the utility of the Washington C filter to find Multiple Populations in NGC 1851 getting very good results using a telescope of only 1 meter aperture, in particular the Swope Telescope at Las Campanas Observatory.

What they found was a spread in the RGB, with a main locus and a relatively small number of stars dispersed to the red. Also he made an study in the MS finding evidence of a similar color distribution there as well. In addition, their analysis of radial distributions found a significant difference between the blue and red MSs(p-value=0.0), with the latter being more centrally concentrated. All these studies were consistent with previous studies in NGC 1851, like Zoccali et al. (2009)

Thus, this system provides a good ground-based alternative to the heavily over-subscribed Hubble Space Telescope. Our goal in this investigation is to search for Multiple Populations in another Globular Cluster, NGC 7099 (M30), further investigating the utility of the Washington system to uncover MPs, again taking advantage of the system's efficiency to undertake this study using in large part only a 1m telescope.
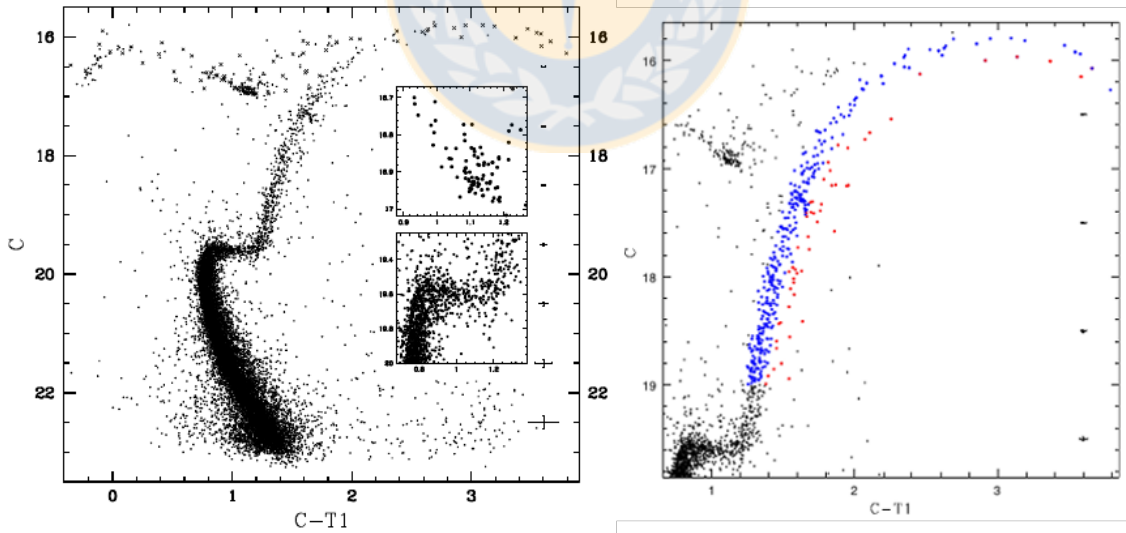
Figure 19: At left: CMD of NGC 1851 using $C-T_1$ vs C, the HB and SGB have been zoomed. Right: a zoom to the RGB clarifying the redder and bluer populations. Source: Cummings et al. (2014)

3.4 NGC 7099 (M 30)
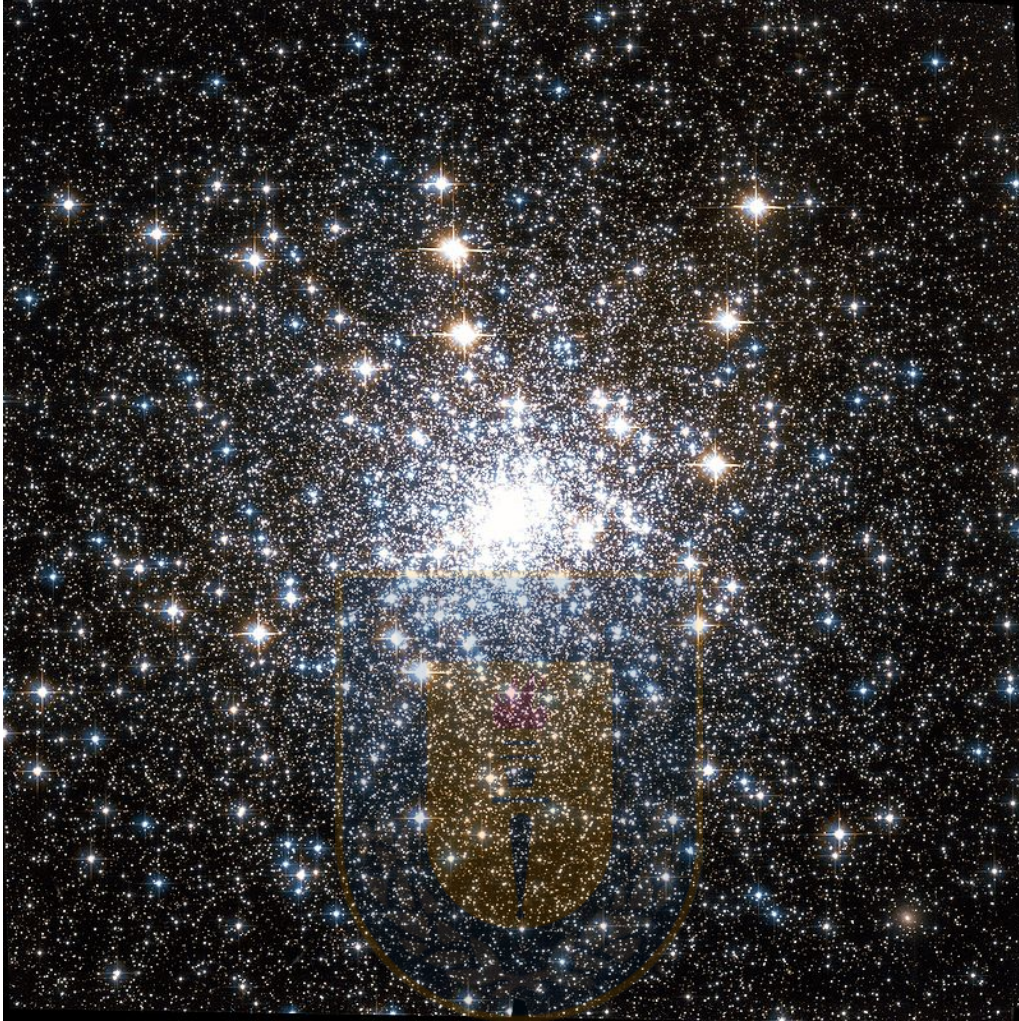
Figure 20: NGC 7099 (M30). Source: http://freestarcharts.com

This very metal poor cluster([Fe/H]= -2.27) is situated in the galactic halo at 8.1 Kpc from our Sun, with coordinates(epoch J2000):

$$RA : 21^h \, 40^m \, 22.12^s$$

$$Dec : -23° \, 10' \, 47.5''$$

its integrated V magnitude is 7.19 and it has a foreground reddening of only 0.03.(Harris 1996 (2010 edition)) This last information was the reason of why we chose this cluster, because it means that differential reddening corrections are not needed. Also, at the time we took the observations, little other work had been done photometrically on MPs in this cluster, which is also among the most metal-poor in the Galaxy.

It has an estimated age of 12,9 Gyrs(Forbes & Bridges(2010)) and a mass of 1.6×10^6 Solar Masses (Vande Putte & Cropper (2009)); making it a massive cluster and thus one that should fall within Valcarce and Catelan case 2 or possibly 3.

Previous work in this GC concerning MPs was made by Carretta et al. (2009) using 29 RGB stars who found spectroscopically a [Na:O] anticorrelation, showing the presence of MPs.(Figure 21)
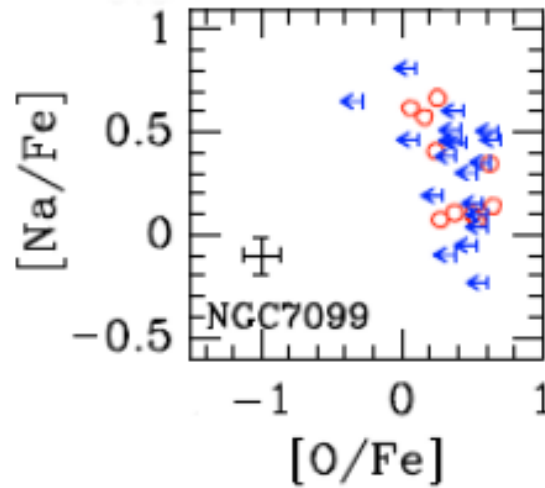
Figure 21: Plot from Carretta et al. (2009) The sample of 29 stars shows a [Na:O] anticorrelation. Source: Carretta et al. (2009)

We saw before, that photometrically Piotto et al. (2015) analyzed 57 GCs using the magic trio of filters (F275W, F336W and F438W) using data from the HST. These studies included NGC 7099. Although their CMD didn't show the typical split of the sequence, it does show a very broad Red Giant Branch. Unfortunately, their study was only limited to make the CMD and no other studies like radial distribution comparisons or estimates of the ratio of FG/SG stars were made.
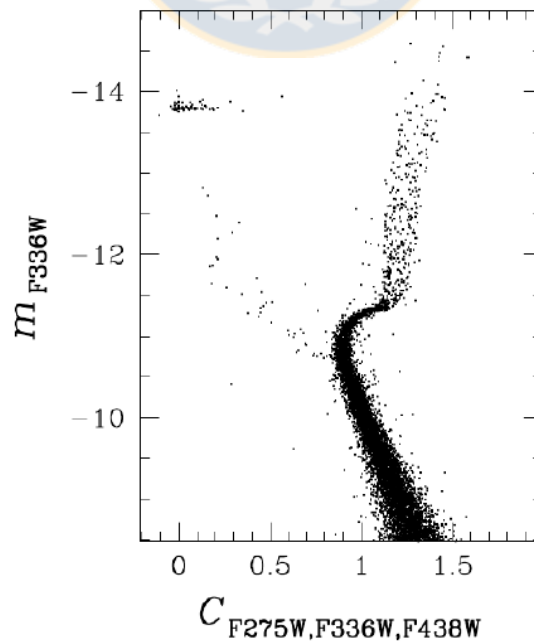
Figure 22: Color-Magnitude Diagram from Piotto et al. (2015). The RGB is very wide, indicating the presence of MPs. Based on data obtained by the Hubble Space Telescope. Source: Piotto et al. (2015)

4 The Data

4.1 The Observations

The data consist of 26 images of which 6 were obtained with the 4m SOAR telescope in 2014 and 20 were obtained with the 1-meter Swope telescope from Las Campanas Observatory. 14 of these images are from 2013 and 6 are from 2011. The SOAR detector(SOI) consisted of a total of 4096 x 4096 pixels at 0.0767 "/pix and a field of view of 5.26 x 5.26 arc minutes, divided into two CCDs with two amplifiers each resulting in 4 columns of 1024x4096 pixels. The Swope telescope worked with only one CCD (SiTe3) of 2048x3150 pixels at 0.435 "/pix and a field of view of 14.9 x 22.8 arc minutes. The filters used for this work were the Washington C filter, and the filters R and I in replacement of the Washington filters T_1 and T_2. Geisler (1996) demonstrated that the filter R_{KC} is a more efficient and very good substitute for T_1. Aditionally, the T_2 filter is almost identical to the I_{KC} (Canterna 1976; Geisler 1996). We obtained 5 images each in R and I and 10 in C from the Swope, while only C data were obtained with the SOAR telescope, for a total of 16 in C, which is the crucial filter for detecting MPs but also the most difficult to obtain high S/N, especially for red giants. table 2 provides details of the exposures:

	Swope	SOAR
C	1(30s), 3(300s), 6(1200s)	4(10s), 2(300s)
R	1(10s), 1(100s), 3(400s)	-
I	1(10s), 1(300s), 3(1200s)	-

Table 2: Time exposures and number of images per filter. Source: Own elaboration.

The 2011 Swope images have a FWHM of 1.09"-2.23" and an airmass of 1.194-1.406, the 2013 Swope images have a FWHM of 0.96"-1.7" and an airmass of 1.006-1.123, while the 2014 SOAR images have a FWHM of 0.41"-0.53" and an airmass of 1.01. The first night of the 2013 observations was deemed photometric via visual estimate of the sky conditions and we observed a number of standard fields from Geisler (1996) which were later used to calibrate all of the data. Subsequent detailed reduction and analysis showed that this night was indeed photometric.

4.2 Processing and Reduction

For the processing part the program used was IRAF and its standard tasks like ccdproc. For SOAR images, since there were gaps between the chips we decided to work with each amplifier as a separate image. For all the Swope images we used in addition a nonlinearity correction from Hamuy et al. (2006). The photometry was performed by the DAOPHOT suite of programs(Stetson 1987). Since the center of the cluster is crowded, even using images from SOAR telescope, a Point Spread Function was necessary to perform profile-fitting photometry, using bright, isolated stars to define the correct light profiles and make the best photometry.

We Calculated the PSF using 150-200 isolated and bright stars in each image, first with an initial calculation by the DAOPHOT task ps, a manual refinement by eye, a more accurate refinement with a Fortran program that generate the PSF for all PSF stars and subtract out their neighbors between iterations, and a final
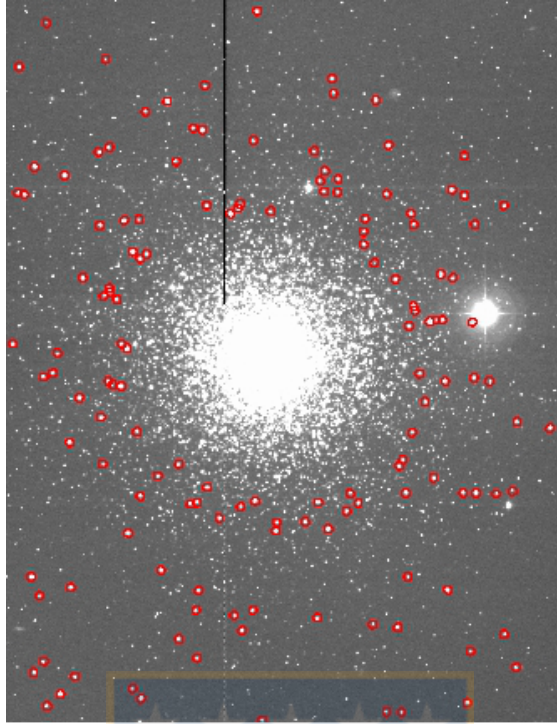
Figure 23: An example of the chosen stars for the Point Spread Function. Source: Own elaboration

refinement using again the DAOPHOT task ps. After that, with a good PSF in hand, we performed the usual 3 passes through find(that looks for all the stars in a frame above a user-defined threshold brighter than the sky), phot(that realizes aperture photometry to all the stars found) and allstar(makes psf photometry and removes the star to find hidden faint stars). Repeating this 3 times allows the most accurate and complete photometry on individual images.

ALLFRAME is a program that makes simultaneous use of the geometric and photometric information from all images of a given field to derive a self-consistent set of positions and magnitudes for all detected starlike objects in that area of sky, thereby extending the range of magnitude and crowding conditions for which useful photometry is obtainable (Stetson 1994). Thus, once all images were done, ALLFRAME was applied to all the images simultaneously, getting the most precise Photometry. Afterwards, the aperture correction was made by comparing the psf photometry of psf stars (with neighbors subtracted out based on the allframe results) to their aperture photometry. DAOMATCH and DAOMASTER were used to match all the short, medium and long images from one filter to get a robust intensity-weighted mean instrumental magnitude, using a medium exposure as a reference image since it has stars in common with short and long exposures facilitating the match.

DAOMATCH makes a first guess of coordinate transformation coefficients by trying to match stars from the 30 brightest stars of each frame.

DAOMASTER makes a more accurate match taking the first guess of DAO-MATCH and refining it, including other functions and options for the match.

Both programs were used again to generate a full catalog with all the stars found in at least 2 of the 3 filters. The R filter was used as reference filter since in the spec-
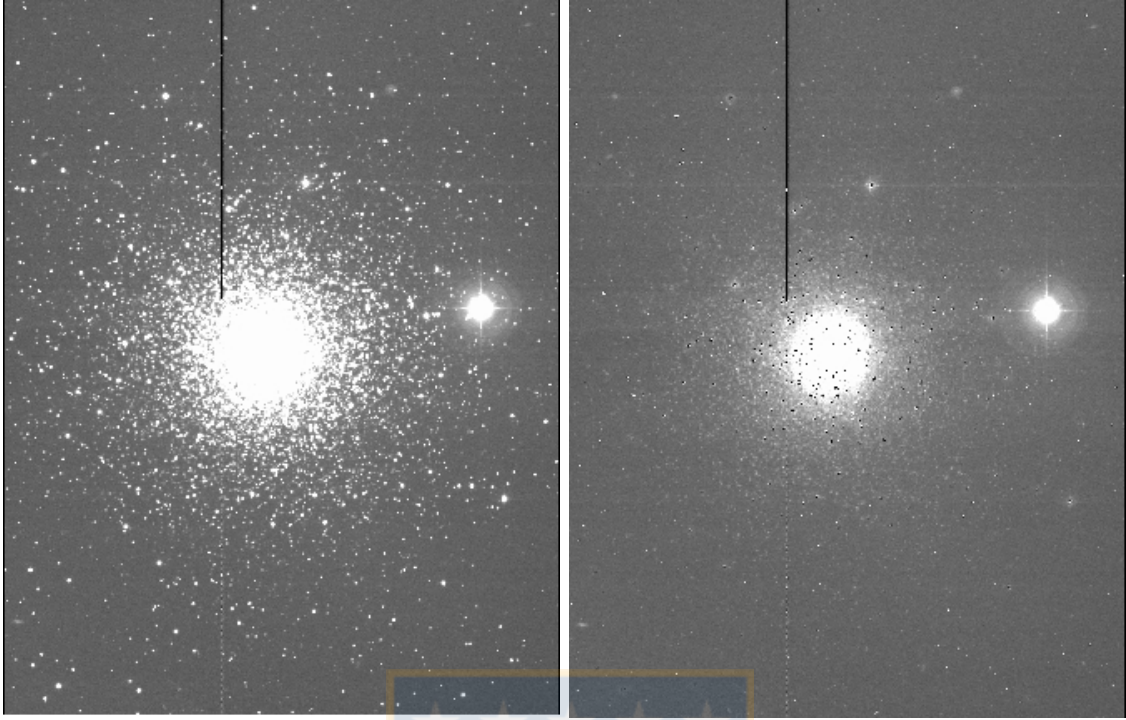
Figure 24: A comparison of the same image before and after allstar(3 times). Source: Own elaboration

trum it is between the C and I filters and because it produces the deepest images. The instrumental magnitudes were transformed to the Standard Washington System using the standard star observations obtained in 2013. This was done by first comparing the observed standards with the ones in Geisler (1996), identifying all the stars, and creating a file with their catalog names, filter, airmass, UT, center star coordinates, magnitude and error. Using this information plus the standard magnitudes in Geisler (1996) in the transformation equations, gave us the zero point(a star that represents a magnitude of 0. So we can then measure the magnitudes of all other stars with respect to this one.), the color term (a term that indicates how much the calibration depends of the color) and the airmass term(indicating how much the calibration depends of the airmass) with a RMS indicating how photometric was the night. It did indeed proved to be photometric. The Details are given in table 3.

	Zero Point	Error	Airmass	Error	Color term	Error	RMS	Sample
C	3.476	0.028	0.288	0.017	-0.021	0.016	0.038	63 stars
R	2.925	0.015	0.074	0.01	-0.092	0.014	0.022	65 stars
I	3.413	0.019	0.04	0.012	-0.003	0.017	0.027	74 star

Table 3: Calibration coefficients: Zero point, airmass and color term, followed by their errors, the RMS and the sample for each filter are also shown. Source: Own elaboration

These coefficients were used with the transformation equations to the program star instrumental photometry to generate the calibrated star catalogue.

The final standardized photometry is given in Table 4. After each magnitude there are two errors (i.e. eX and dX where X is a filter). The first is a statistical assessment of the psf-fitting error for each detection of a star returned by Allframe, in which the reported error is the weighted mean of the errors of the individual detections, where the weight is inversely proportional to the individual error. The second error measures the variation in magnitude(dispersion) of the various independent detections. Note that observations in the R and I filters have been transformed to T_1 and T_2.

| ID	X	Y	C	eC	dC	T_1	eT_1	dT_1	T_2	eT_2	dT_2	nC	nT_1	nT_2
5023	1121.36	1423.45	21.050	0.013	0.028	20.123	0.026	0.043	19.684	0.024	0.053	9	3	3
5034	1223.40	1423.21	19.388	0.005	0.025	18.736	0.017	0.007	18.339	0.022	0.067	15	3	3
5059	775.29	1424.86	20.300	0.006	0.048	19.549	0.022	0.087	18.995	0.027	0.052	15	3	3
8204	1305.69	1532.06	22.356	0.02	0.059	20.951	0.035	0.012	20.315	0.036	0.047	13	3	3
8232	1286.33	1532.12	18.73	0.005	0.047	18.038	0.012	0.007	17.633	0.015	0.017	15	3	3
8277	955.17	1532.24	21.93	0.029	0.342	20.566	0.109	0.197	19.769	0.14	0.133	13	2	3
8229	746.71	1532.25	21.424	0.01	0.018	20.109	0.028	0.048	19.582	0.025	0.036	14	3	3
8238	502.19	1532.28	20.013	0.009	0.024	19.278	0.013	0.011	18.876	0.015	0.01	9	3	3
8251	1188.42	1532.39	21.182	0.013	0.074	20.048	0.031	0.033	19.522	0.039	0.009	15	3	3
8216	1011.44	1532.41	20.047	0.022	0.324	18.994	0.051	0.034	18.315	0.063	0.208	9	3	3

Table 4: The columns are: ID, X and Y coordinates, magnitude, error and dispersion in C, T_1 and T_2, and the number of frames where the star was detected in C, T_1 and T_2. Source: Own elaboration

5 The Analysis

5.1 Addstar experiment

In order to determine the best estimate of the true internal photometric errors, we performed Addstar experiments using the eponymous DAOPHOT task. This consisted in adding random fake stars (in magnitude and position) to one frame for each filter. We then performed exactly the same photometry process as described above and then determine the difference in magnitude between the input and output values. This difference we take as our best estimate of the real internal photometric error (neglecting errors in the transformation which will affect all stars equally). For this test, we added no more than 10% of the original number of stars photometered in a frame (i.e. For the C long image that had 17405 stars, we created 1740 fake stars) and repeated the process 10 times, thereby measuring in the end the same number of stars as actually in the image.

In figure 25 we can see a comparison in each filter between the internal errors reported by Allframe with the addstar error. For brighter magnitudes both errors are similar, with the addstar errors spreading to 0, while for fainter magnitudes the spread of the addstar errors become greater. In both cases these errors are in reasonable agreement throughout the magnitude range so we will therefore just use the internal error as our best estimate for each star. The similarity of the errors encourages us that allframe does a very good job at both measuring the star's flux as well as determining its error.
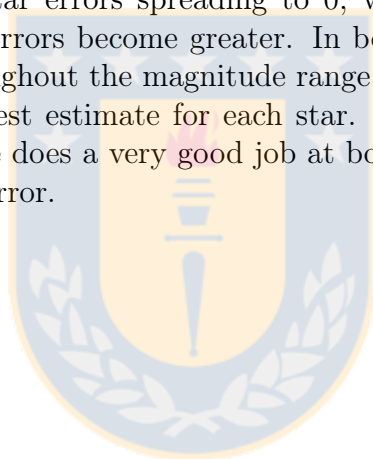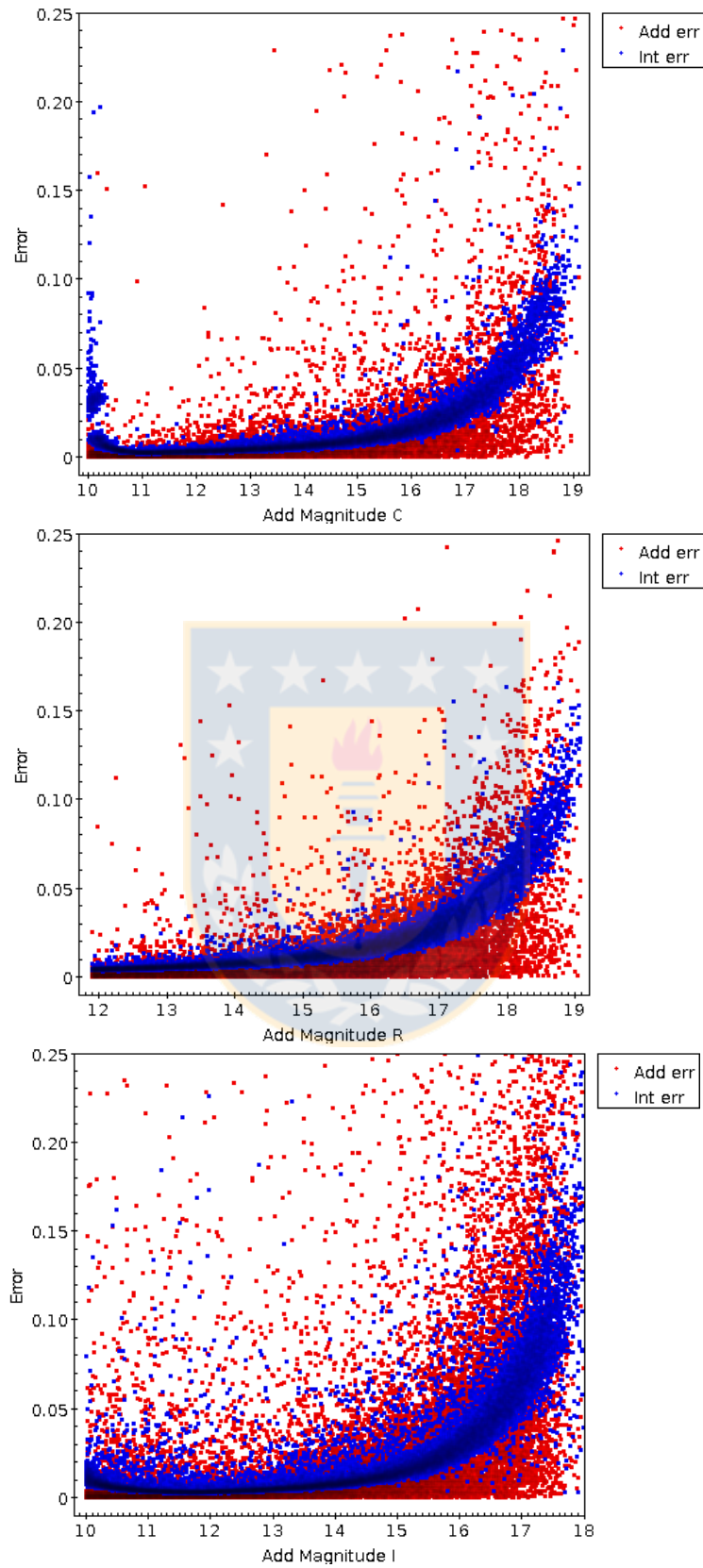
Figure 25: Plots of magnitude vs error, The red points are addstar errors and the blue points are internal errors. The two are in reasonable agreement in general so we will use the internal Allframe error as our photometric error. Source: Own elaboration

We also plot in Fig. 26 the completeness as a function of magnitude based on the Addstar experiments. The 50% completeness level is found to be 17.9 for the C filter, 18.1 for R and 17.5 for I. The difference among the completeness of these filters is due to the different broadband and responses of each one.
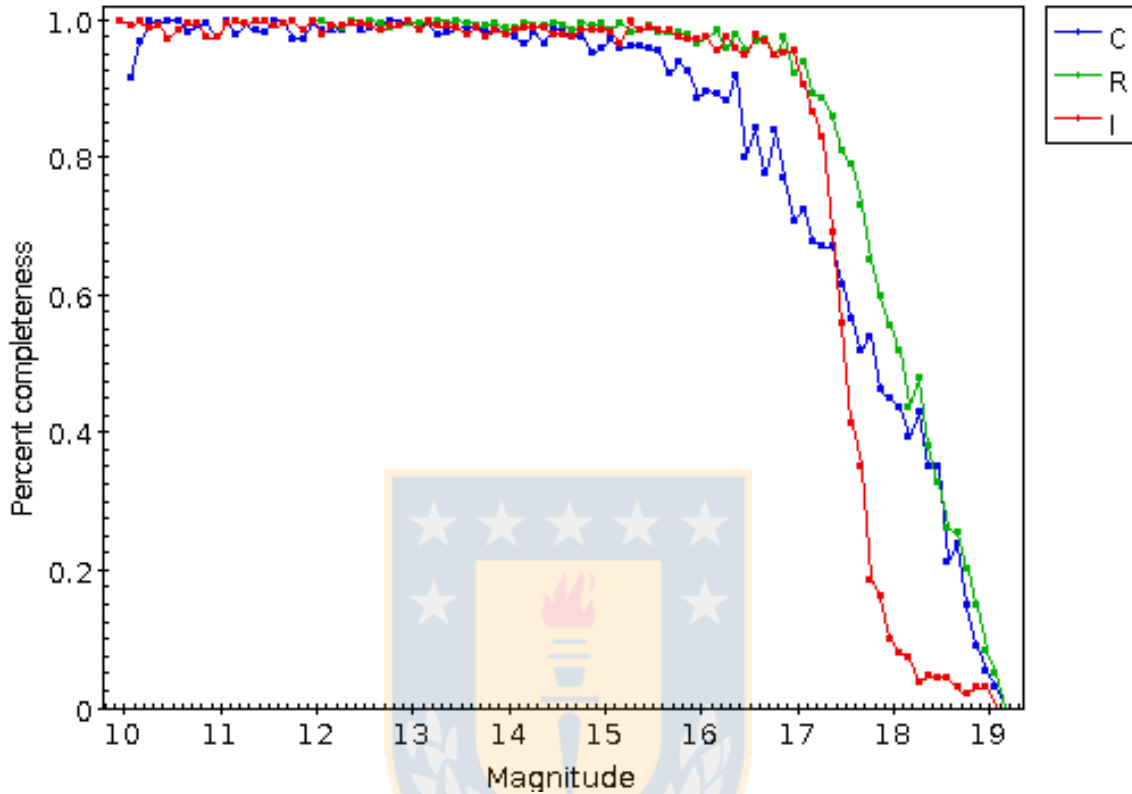

Figure 26: Plot of completeness as a function of magnitude based on the Addstar experiments. Source: Own elaboration

Also we made another plot of completeness but this time as a function of radius, using only the images from the Swope telescope. This plot (Fig. 27) shows that there were almost no stars found inside a radius of 100 pixels from the center of the cluster due to extreme crowding. Even in the outer parts, the curves don't reach near 100% completeness due to the faint stars that aren't found, as seen in the previous plot of Completeness as a function of magnitude.

We thus decided to eliminate this innermost region from subsequent study. Another analysis was made later that included SOAR images. This is described in section "Revealing Multiple Populations". So we now have in hand definitive estimates of the errors and completeness and their variation with magnitude and radius which are required to make the best analysis concerning MPs.
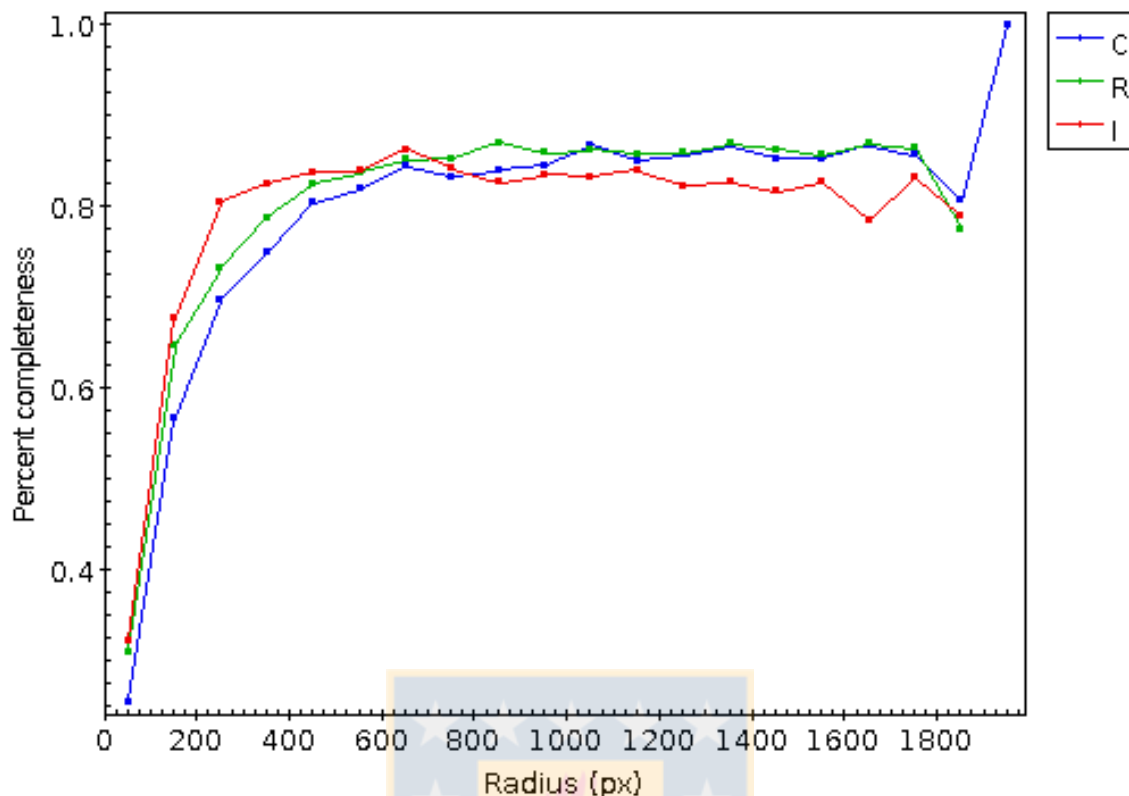
Figure 27: Plot of completeness as a function of Radius based on the Addstar experiments. Source: Own elaboration

5.2 Error analysis

As said before there are two kind of errors in Table 4. The first(i.e. eC) being a statistical assessment of the psf-fitting error for each detection of a star returned by Allframe, in which the reported error is the weighted mean of the errors of the individual detections, where the weight is inversely proportional to the individual error. The second error (i.e. dC) measures the variation in magnitude of the various independent detections. So if a faint star is found in only one frame this second error would be 0, and we would have no knowledge of the actual internal error, and thus we removed all the stars that were found in only 1 frame in a Filter(The last three columns in the table indicates in how many images appear each star in each filter). As expected, fainter stars generally have larger internal uncertainties and also a larger dispersion among different detections. However, there are also a relatively small number of brighter stars with small internal uncertainties but large dispersions, most likely due to crowding or undetected saturations. We decided to make a combination of both the internal error and the dispersion, using the square root of the sum of both quadratic values. From here on, we refer to this value as the error. We then removed all stars, in separated catalogues according to the color, with an error larger than 0.1. This eliminated very few bright stars and should have negligible effect on our main results, which are limited to brighter stars.

29

5.3   Revealing MPs

With catalogues for each color containing only stars well measured and with small errors (a total ~ 15000 in each catalogue) we now proceeded to make various CMDs including $C - T_1$ vs T_1, $C - T_1$ vs C, $C - T_2$ vs C, and $T_1 - T_2$ vs T_1. However, before making the CMDs, we further cull our dataset to maximize the scientific return by first statistically correcting for field stars and investigating crowding. From our addstar experiment we knew that very few stars within 100px of the center on the Swope images were found and could be well measured. However, we can further investigate the radial behavior by adding the SOAR images. We divided the central region of the catalogue including SOAR images into annuli with a width of 10px and noticed that beyond a radius of 50px the dispersion dropped significantly. We thus set 50 Swope px as the inner useful radius. Similarly, by investigating the structure and dispersion of the various parts of the CMD we determined that field stars were most effectively removed by establishing a maximum cluster radius of 1000 Swope px. The CMD beyond this radius shows no distinguishable RGB, which is the main focus of our investigation, so we lose a negligible fraction of these stars by using this limiting cluster radius.

Figure 28 shows the four distinct CMDs using different combinations of our 3 filters. As said before, each CMD has its own catalogue with all the stars with color errors higher than 0.1 removed, without affecting the other CMDs. Black errorbars have been put representing the mean in each magnitude bin(i.e. the error in 15.5 is a mean of all the errors between magnitude 15 and 15.999) as said before, these errors were determined using the square-root of the quadratic sum of the dispersion and internal error of each star. **All 3 CMDs involving the C filter show an intrinsic color spread on the mid to lower RGB, larger than that expected from photometric errors alone, while the T_1 vs $T_1 - T_2$ CMD color spread is consistent with no intrinsic variation.** This is exactly the behaviour expected if NGC 7099 contains MPs, because filter C is very sensitive to the differences in flux of the molecular bands of first and second generation stars, but T_1 and T_2 don't have such sensitivity, making MPs indistinguishable.

Due to reddening being very small (E(B-V)=0.03), differential reddening is assumed to be negligible. Actually $E(C - T_1) \sim 2 \times E(B - V)$, giving a value of $E(C - T_1) = 0.06$, but this value is still very small. And of course here we are only interested primarily in relative photometry, and the negligible variable reddening means that our main results are not affected by reddening. Note that, unlike the case in NGC 1851 and typical Washington photometry, the C photometric errors are actually smaller than those in the redder filters, specially T_2 due to the fact that we had a large number of long exposures with the Swope and especially because of the SOAR images, using a 4m telescope, which were only obtained for C.

The net effect is to produce photometric C errors which are quite small and clearly much smaller than the color spread we see in this part of the CMD. In particular, there are a number of stars that scatter well to the blue of the main RGB ridgeline. The behavior in the different filters leads us to conclude that the cause of this spread is most likely due to Multiple Populations. Also, every diagram has error bars inside the RGB and MS to demonstrate that this spread to the blue in the RGB is very unlikely due to errors. Note that the errorbars cover the main locus of the RGB in all cases, but in the diagrams with C they are too small to reach the stars to the left of the RGB.
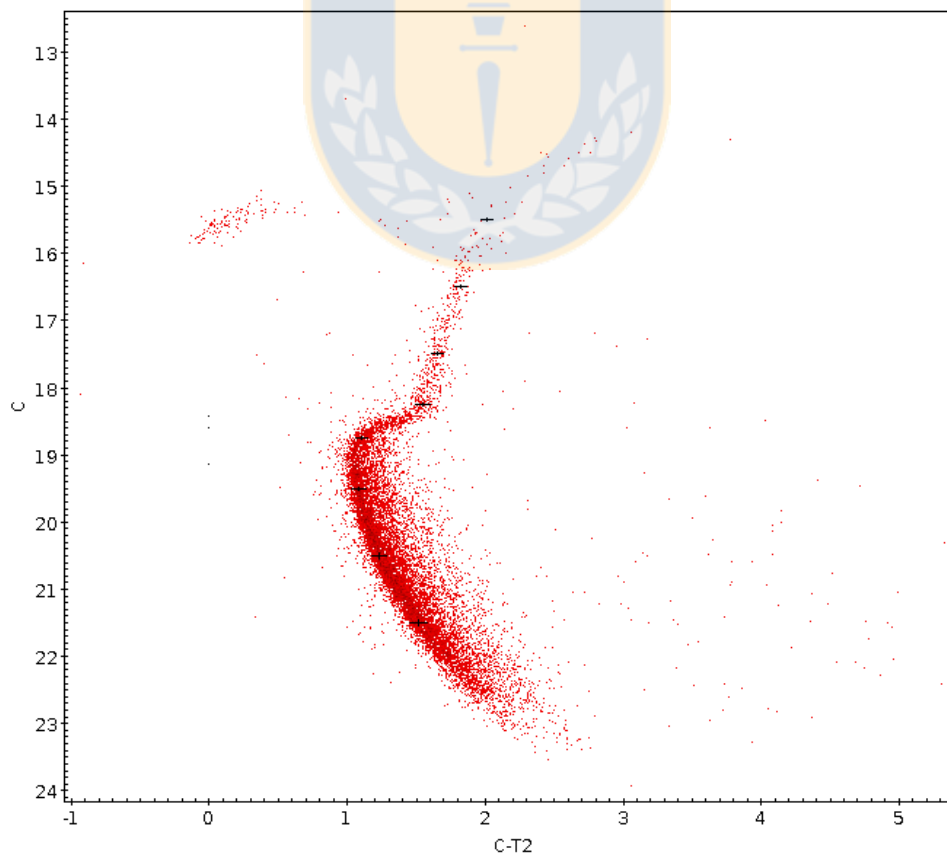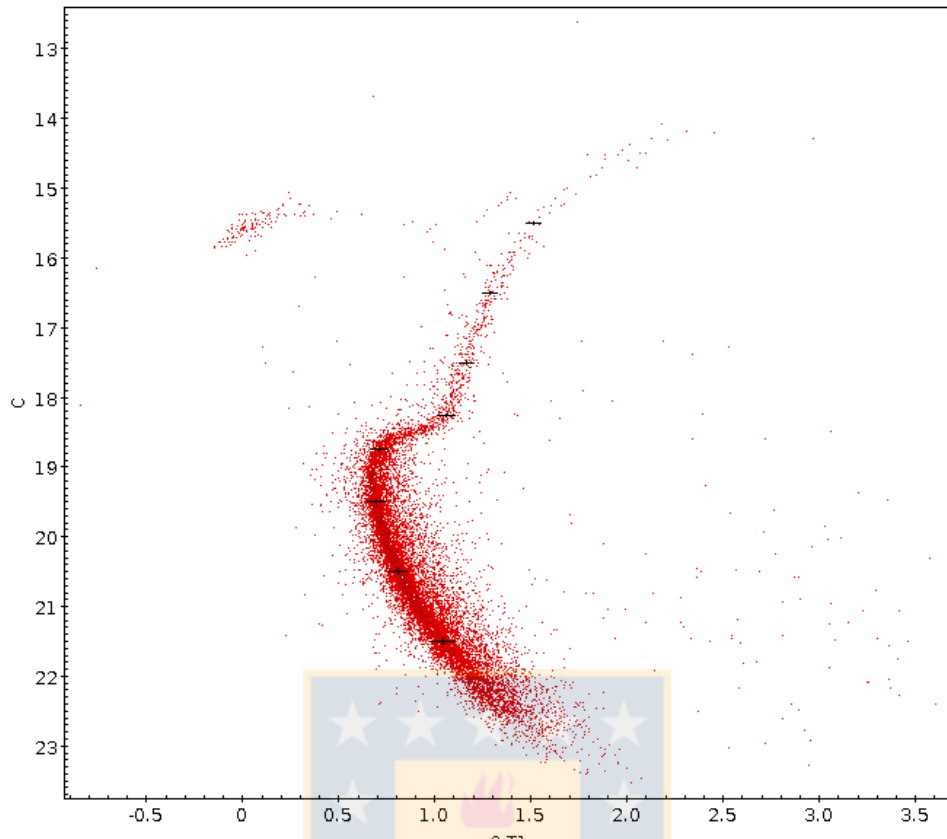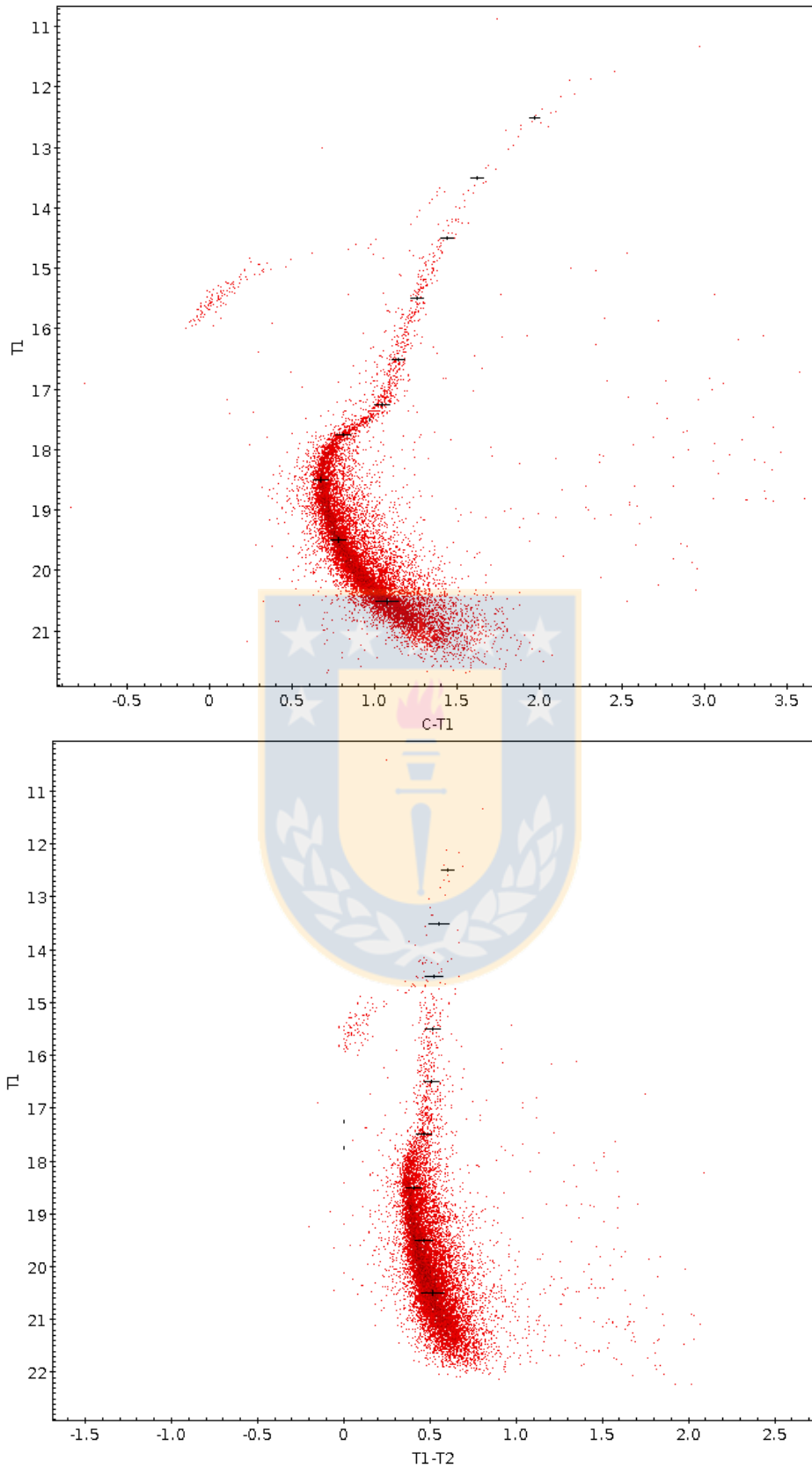
Figure 28: Four CMDs. Errorbars corresponding to the mean error (see text for details) determined in 1 mag bins have been put along the sequences. All 3 including the C filter show significant intrinsic color spreads along the mid to lower RGB, most notably by a scattering of stars to the blue of the main RGB locus. While the T_1 vs $T_1 - T_2$ CMD has a spread consistent with that expected from photometric errors alone. Source: Own elaboration
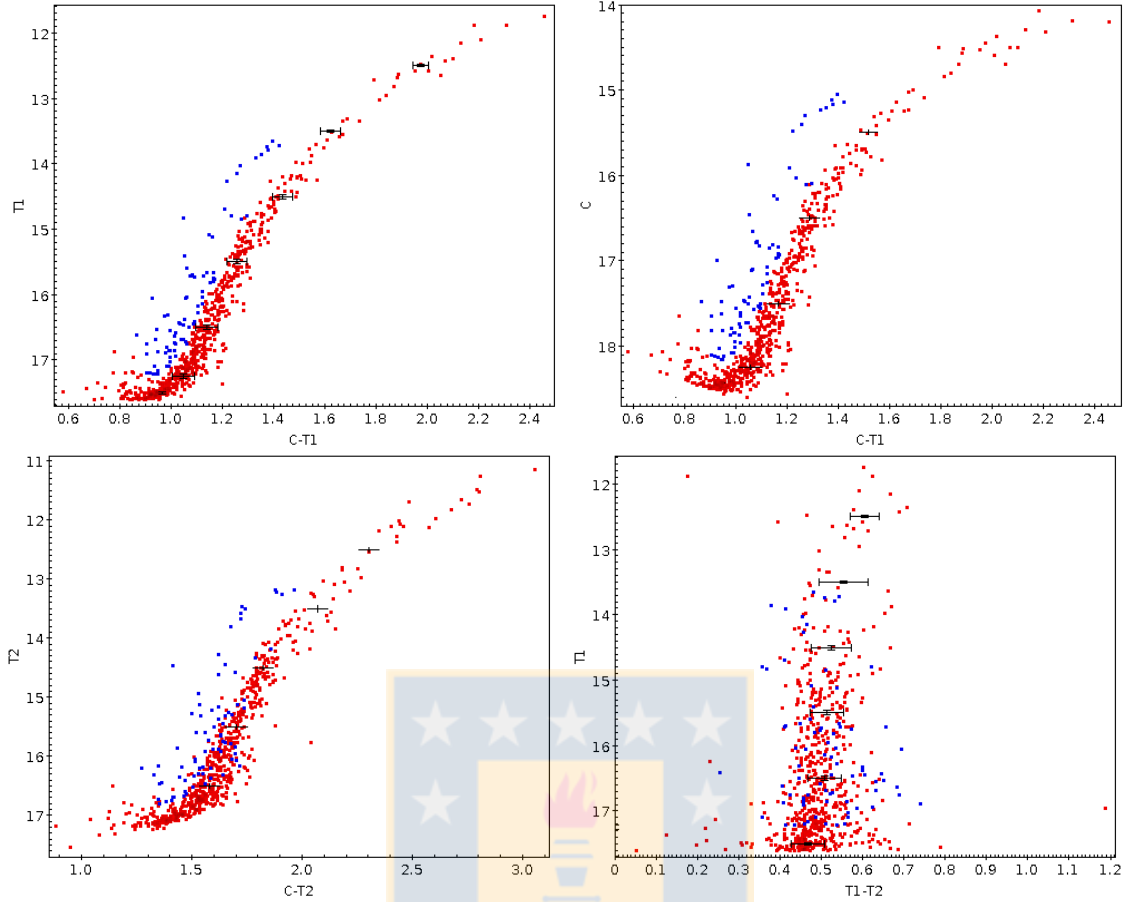
Figure 29: Zoom in on the RGB. The two diagrams on the top and the bottom-left include the C filter while the bottom-right does not. We used the T1 vs C-T1 CMD to define the blue and red stars and then applied this to the other CMDs (very bluest were already deleted as $> 4\sigma$ outliers). These same stars appear in blue in the other 2 CMDs involving the C filter as well. In the T_2 vs $C - T_2$ CMD, these stars again appear generally bluer than the main RGB. However, in the T_1 vs $T_1 - T_2$ CMD, these stars fall along the main RGB. Source: Own elaboration

Figure 29 shows a zoom to the RGB. We color code in blue stars that lie to the blue of the main RGB locus in the T1 vs C-T1 CMD. We use this same color for these stars in the other CMDs.

$C - T_1$ are the clearest Diagrams showing this spread, $C - T_2$, although is not as clear as $C - T_1$ still shows a clear spread and most of the stars remain at the bluer side, but $T_1 - T_2$ has these stars completely mixed with the RGB. This occurs because while the filter C is very sensitive to the differences in flux of the molecular bands of first and second generation stars, T_2 covers only a little difference in flux in the far red CN band, allowing a separation of first and second generation stars in the CMD using $C - T_2$. While the filter T_1 doesn't cover any significant difference in the flux of first and second generation stars, making a bigger separation of them when using $C - T_1$ in a CMD. This is another evidence for the Washington C filter being excellent in the search for MPs.

Another test was made. We fitted a fiducial curve for the RGB in $C - T_1$ vs T_1 and $T_1 - T_2$ vs T_1 between magnitudes 15.5 and 17.5, making a Histogram with the fiducial(defined as the highest density locus of stars along the RGB) and deriving
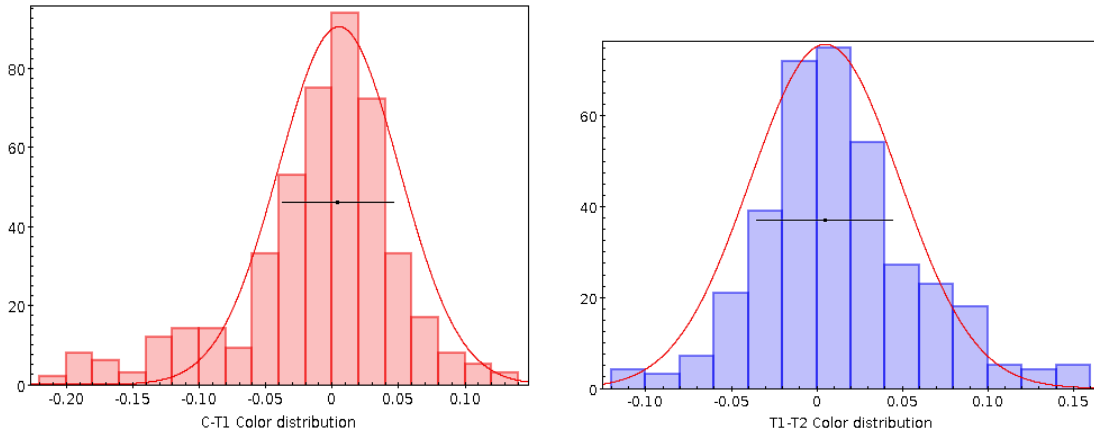
Figure 30: Color Distributions for the RGB in $C-T_1$ and T_1-T_2. Mean photometric errors of each RGB are indicated as black horizontal lines. Source: Own elaboration

the color distribution from it. In addition we calculated statistically the best fit gaussian for both histograms (Fig 30). We dropped 12 stars in $C-T_1$ that were $> 4\sigma$ from the respective fiducial because we considered them as true outliers, although note that this makes our results conservative and that there is a possibility that these stars are indeed extreme MP stars. Note that most of these stars were also to the blue of the main RGB locus. All the other stars inside this range were considered for this study. The result was that for $T_1 - T_2$ the Gaussian was well fitted and the FWHM(0.043) very comparable to that expected given the mean photometric errors(0.040) indicated as a black line at the middle of the histogram, but for $C - T_1$ the gaussian fit, that has a FWHM of 0.045 compared to photometric errors of 0.042, is poor and we see an extension to the left. These stars satisfy all the requirements to be considered as a different population of those inside the Gaussian.

All this evidence suggests that we have a small bluer stellar population different from the main population on the RGB.

These results are in rough agreement to the findings in Piotto et al. (2015), showing a significant spread in the RGB(Figure 22), but should be added that in his case the RGB doesn't show a main locus as seen in our studies, but an homogeneous spread along the RGB. Looking to figure 18, the filter C covers a big difference of CN abundance between FG and SG stars, and according to previous studies, described in section "Abundance differences in globular clusters" the CN strength is smaller in FG stars than SG. Meaning that we expect a higher flux(hence smaller magnitude) in the filter C from a FG star than SG star, but similar fluxes in filter T_1. Resulting in a FG star being bluer than a SG star. That means, our bluer population is expected to be the FG. This is a very interesting result since extrapolating to the entire cluster it would represent only about 20% of the Cluster. It is opposite to the results of Cummings et al. (2014) in NGC1851, who found a FG being the $\sim 70\%$ of the cluster. However, as said before, Caretta et al.(2009) find that generally SG stars make up roughly 2/3 of the current cluster population, in rough agreement with our finding.

34

5.4 Radial Distributions

There is an intense debate about whether the different populations have significantly different radial distributions or not. Studies concerning NGC 1851, Zoccali et al. (2009) and Carretta et al. (2011) argue that different populations on the RGB have differing radial distributions, with the redder population more centrally concentrated, Milone et al. (2009) and Olsewski et al. (2009) didn't find any evidence. Cummings et al. (2014) didn't find a meaningful difference in the radial distribution of the RGB(p-value=0.55) in NGC 1851, but they recognized that their small sample limits the analysis, while a larger sample in the MS gave them a very significant difference in the radial distributions (p-value=0.0), indicating a redder population more centrally concentrated, and supporting Zoccali et al(2009) and Carretta et al.(2011) arguments. More evidence indicating different radial distributions are found in Lardo et al. (2011) who studied 9 GCs, finding significant color spreads and a more concentrated redder population in 7 of them, while Johnson & Pilachowski (2012) found different radial distributions in NGC 6205, with the redder population being again more centrally concentrated.

Other studies like Dalessandro et al. (2014), found a fully spatially Mixed FG and SG in NGC 6362, however they recognize that is the first evidence found of such behaviour in GCs.
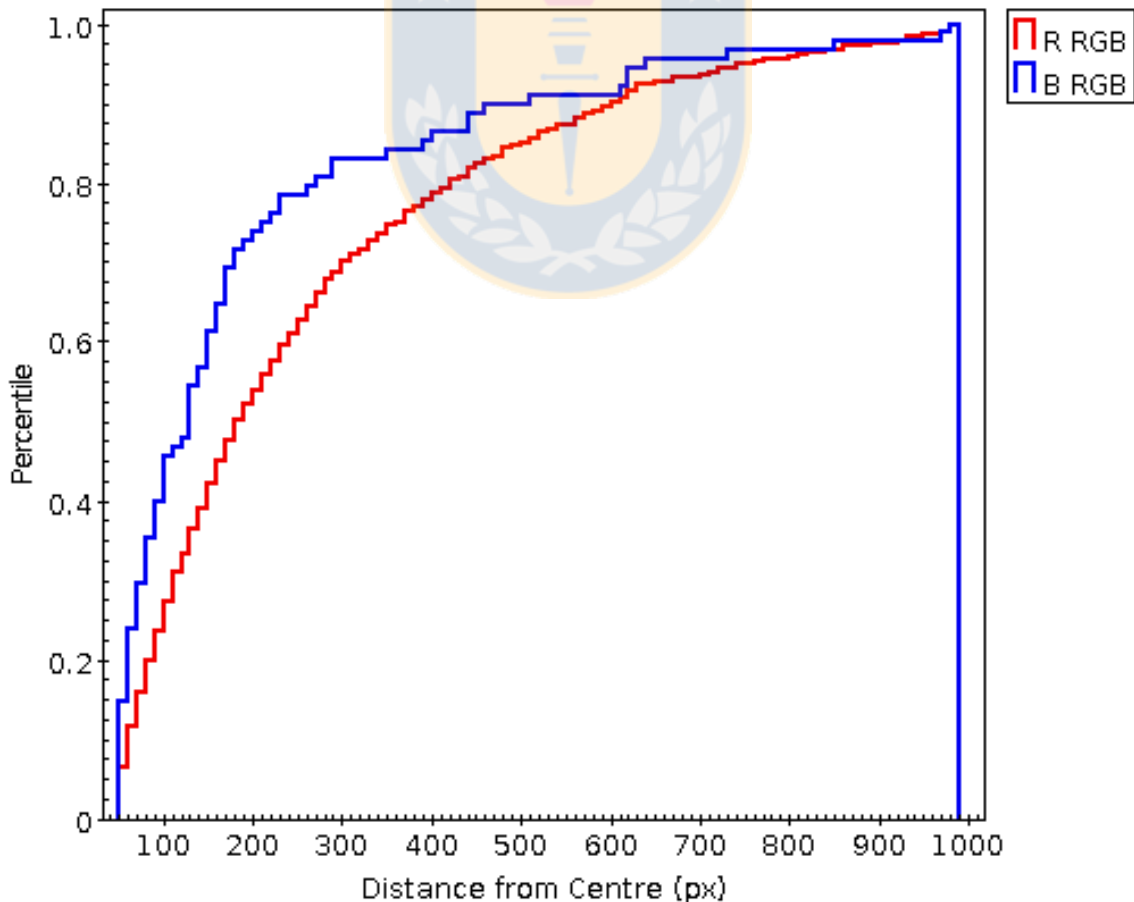

Figure 31: Radial distribution comparison between the bluer and redder RGB in NGC 7099. Source: Own elaboration

Figure 31 shows a comparison of the NGC 7099 radial distribution between the bluer and redder RGB. By looking at the left histogram in figure 30, we defined $C - T_1 = -0.06$ as the limit between bluer and redder RGB stars and divided the sample in two different subsets. Clearly the graph shows a blue line rising faster than the red line, meaning a bluer population more centrally concentrated, opposite to the typical case where is the redder population which present this behaviour.

A Kolmogórov-Smirnov test was made to find if this difference in the radial distribution between these two populations was significant or not. We found a very statistically significant difference ($p - value = 0.0$), meaning that the distributions are intrinsically distinct at essentially the 100% confidence level.

This is an interesting but unexpected result because, indeed, we expected a different radial distribution between both populations, but it is generally found that the SG, not the FG, stars are more concentrated.

Most of the formation scenarios cited in this work show SG stars being formed in the center of the cluster. Until now, to our knowledge this is the first indication of the FG being more centrally concentrated than the SG. Our result seriously defies these scenarios generating a discussion exposed in the next section. Unfortunately Piotto et al. (2015) didn't make a radial analysis of NGC 7099, and at present no similar studies have been made of this cluster. Such studies would be of great interest to see if they confirm or negate our results.
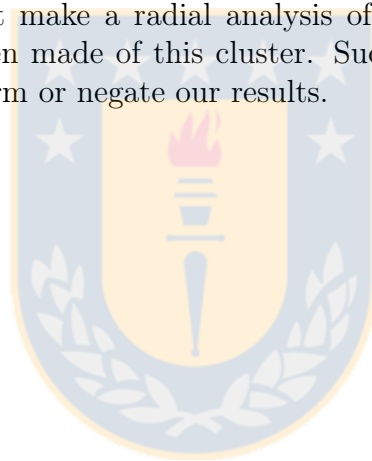
6 Conclusions and Discussion

In the previous sections we have studied the utility of the Washington C filter for studying MPs. As first shown by Cummings et al. (2014), this filter is very efficient at detecting MPs in the first test case - NGC 1851, showing MPs based on photometry obtained from a 1m telescope. We have used the same telescope to investigate a second cluster - NGC 7099. And indeed it allowed us to do a variety of studies concerning the search of MPs. This opens a very good option for studying MPs from ground based telescopes, especially in the near future when, after the imminent demise of HST, we will be left UV-blind, so that, e.g., 2 of the "magic trio" of UV HST filters used by Piotto et al.(2015) to study in great detail MPs in a variety of GCs, will not be available.

We found a real spread along the RGB in all the CMDs that included the C filter, with $C - T_1$ showing most clearly both populations, $C - T_2$ still differentiated them substantively, but $T_1 - T_2$ showed no significant intrinsic spread, mixing both populations in the RGB. The spread displayed in $C - T_1$ and $C - T_2$ was manifested by a significant number of stars lying significantly bluer of the main red giant locus, with a color spread much larger than that expected from the photometric errors, which were well determined from addstar experiments. All these evidence indicates and suggest that there exist MPs in NGC 7099, agreeing with previous photometric and spectroscopic studies. Interestingly, we find that the bluer population, expected to be FG stars, is only about 20% of the total population of the cluster. However, our most intriguing finding is with respect to the radial distribution of the MPs. The radial distribution of both populations showed to be significantly different being consistent with the position of Zoccali et al. (2009) and Carretta et al. (2011). But contrary to the expected results, namely that the redder population should be more concentrated, our evidence shows a more concentrated bluer population instead. This fact contradicts most of the actual formation scenarios for MPs. Of course, as noted above, currently there is no scenario which can account for all of the observations.

Valcarce and Catelan (2011) explained in their theory (seen in this work in section "Formation scenarios for MPs") the possible formation scenario of NGC2808 (intermediate-mass PS). NGC 2808 has a mass of 1.4×10^6Solar masses(Boyles et al. (2011)), a very similar mass to NGC 7099(1.6×10^6). Thus, we might expect that NGC 7099 might also present three populations. We hypothesize that our finding that the bluer population is more concentrated suggests that it was formed after the main redder population and may correspond then to the Valcarce and Catelan purported third population, with the redder one corresponding to their second population. One is then left needing to explain what happened to the first generation. It is of course very unlikely that any purported first generation has disappeared completely. Note that both the Carretta et al spectroscopic and the Piotto et al. photometric data show no strong hints of distinct populations, but instead rather continuous distributions, with no strong concentration of stars along the sequence. Our data on the other hand do suggest a preponderance of redder stars with a scattering to the blue.

Our result adds to the growing amount of data characterizing MPs. Unfortunately, as noted above, no current theory is able to explain satisfactorily the wide variety of behavior that MPs display. Our result indeed increases this complexity.

Finally, we can conclude that more studies in NGC 7099 and other GCs are needed. A more detailed spectroscopic study of NGC 7099 would help to clarify our results. The analysis of radial distributions in other globular clusters should continue to be explored to see if any other clusters display the same behaviour. Additional photometric studies are especially useful in this regard and we have confirmed that the Washington system is a very efficient alternative for studying MPs.

7 Bibliography

- Schneider & Arny. (2014) Pathways to astronomy Units 69,71

- Eric Chaisson, Steve McMillan. (2004). Astronomy today.

- Kaufmann, William J. (1991). Universe.,3rd Edition, W.H. Freeman

- WISE Data Processing
  http://wise2.ipac.caltech.edu/docs/release/prelim/expsup/sec4_3c.html

- W. Romanishin.(2000) An introduction to astronomical Photometry using
  CCDs http://www.nhn.ou.edu/ wjr/research/wrccded2.pdf

- Baade, W. 1944, ApJ, 100, 137

- Bastian, N. 2015, arXiv:1510.01330

- Bedin, L. R., Piotto, G., Anderson, J., et al. 2004, ApJL, 605, L125

- Bessell, M. S. 2005, ARAA, 43, 293

- Boyles, J., Lorimer, D. R., Turk, P. J., et al. 2011, ApJ, 742, 51

- Brown, J. A., Wallerstein, G., & Zucker, D. 1997, AJ, 114, 180

- Canterna, R. 1976, AJ, 81, 228

- Carretta, E., Bragaglia, A., Gratton, R. G., et al. 2009, A&A, 505, 117

- Carretta, E., Bragaglia, A., Gratton, R. G., et al. 2010, A$A, 516, A55

- Carretta, E., Lucatello, S., Gratton, R. G., Bragaglia, A., & D'Orazi, V. 2011,
  A&A, 533, A69

- Cohen, J. G. 1978, ApJ, 223, 487

- Cottrell, P. L., & Da Costa, G. S. 1981, ApJL, 245, L79

- Cummings, J. D., Geisler, D., Villanova, S., & Carraro, G. 2014, AJ, 148, 27

- Dalessandro, E., Massari, D., Bellazzini, M., et al. 2014, ApJL, 791, L4

- D'Ercole, A., D'Antona, F., Ventura, P., Vesperini, E., & McMillan, S. L. W.
  2010, MNRAS, 407, 854

- D'Ercole, A., Vesperini, E., D'Antona, F., McMillan, S. L. W., & Recchi, S.
  2008, MNRAS, 391, 825

- Forbes, D. A., & Bridges, T. 2010, MNRAS, 404, 1203

- Geisler, D. 1996, AJ, 111, 480

- Hamuy, M., Folatelli, G., Morrell, N. I., et al. 2006, PASP, 118, 2

- Harris, W.E. 1996, AJ, 112, 1487

- Hénault-Brunet, V., Gieles, M., Agertz, O., & Read, J. I. 2015, MNRAS, 450, 1164

- Ideta, M., & Makino, J. 2004, ApJL, 616, L107

- Johnson, C. I., & Pilachowski, C. A. 2012, ApJL, 754, L38

- Koleva, M., Prugniel, P., Ocvirk, P., Le Borgne, D., & Soubiran, C. 2008, MNRAS, 385, 1998

- Lardo, C., Bellazzini, M., Pancino, E., et al. 2011, A&A, 525, A114

- Lee, J.-W. 2010, MNRAS, 405, L36

- Milone, A. P., Marino, A. F., Piotto, G., et al. 2013, ApJ, 767, 120

- Milone, A. P., Piotto, G., Bedin, L. R., et al. 2012, ApJ, 744, 58

- Milone, A. P., Piotto, G., King, I. R., et al. 2010, ApJ, 709, 1183

- Milone, A. P., Stetson, P. B., Piotto, G., et al. 2009, A&A, 503, 755

- Norris, J., Freeman, K. C., & Da Costa, G. S. 1984, ApJ, 277, 615

- Olszewski, E. W., Saha, A., Knezek, P., et al. 2009, AJ, 138, 1570

- Osborn, W. 1971, The Observatory, 91, 223

- Piotto, G., Milone, A. P., Bedin, L. R., et al. 2015, AJ, 149, 91

- Renzini, A., D'Antona, F., Cassisi, S., et al. 2015, MNRAS, 454, 4197

- Sbordone, L., Salaris, M., Weiss, A., & Cassisi, S. 2011, A&A, 534, A9

- Smith, G. H., & Norris, J. 1984, AJ, 89, 263

- Sneden, C., Kraft, R. P., Prosser, C. F., & Langer, G. E. 1992, AJ, 104, 2121

- Stetson, P. B. 1987, PASP, 99, 191

- Stetson, P. B. 1994, PASP, 106, 250

- Valcarce, A. A. R., & Catelan, M. 2011, AAP, 533, A120

- Vande Putte, D., & Cropper, M. 2009, MNRAS, 392, 113

- Villanova, S., Geisler, D., Carraro, G., Moni Bidin, C., & Muñoz, C. 2013, ApJ, 778, 186

- Zoccali, M., Pancino, E., Catelan, M., et al. 2009, ApJL, 697, L22